Instead, we have uncovered a set of grid cells that represent a rapid change in shape. When we encounter a grid cell of this type, then we deform the shape in the grid cell to conform to any adjacent grid cell and assign it to the equivalence class that forces the least amount of deformation.

Two equivalence class shapes may fail to connect in a region where they should. When this happens, we deform the respective shape in those boundary grid cells until they match the tri-linear interpolation function in each grid cell.

We now discuss the interface between two grid cell equivalence classes. If a grid cell face separates the two equivalence classes, then we call the interface "sharp", otherwise the interface is "diffuse". If the interface is "sharp", then there exists a 1D boundary separating the two shapes. We compute this boundary by equating the two quadratic surface expressions and solving. This is not always smooth, so it will be necessary to blend a narrow region on each side of the intersection curve. If the interface is diffuse, then we have a 2D region of overlap between the two shapes in which the smoothing can be naturally accommodated. We fit a shape to the overlap. We close this topic by checking this analysis against two adjacent grid cells that have different conic section fibre bundle shape approximations. We conclude that the analysis is valid, since tri-linear interpolation is continuously differentiable on the grid cell face that separates the two adjacent grid cells.

Now we overlay the patchwork shape on top of the original implicit surface S and look for chances to

reduce the misfit. We will do this by approximating the volume as a 3D Riemann integral. Our misfit reduction procedure is as follows.

Misfit reduction algorithm

1. We project the noisy implicit surface onto the patchwork smooth surface. We identify connected regions of the implicit surface that are responsible for significant misfit and try to reduce these regions first.
2. We anticipate multiple misfit regions associated to each smooth shape. The most complicated element in a misfit description is the representation of the outermost 1D boundary of the misfit. We use the outermost 1D boundary to define a Riemann sum approximation to the misfit. Consequently, we will ignore (initially, at least) low amplitude but high frequency nearby features.
3. Define height field (relative to the smooth approximant) contours at each critical point in the noisy implicit surface. Project these contours onto the smooth approximant.
4. Smooth the set of projected contours. For each contour in the parameterization we identify the critical points on that contour. We triangulate the annular region bounded between consecutive contours.
5. Now we fit a frustum-like collar to the base of the region where the misfit attaches to the background.
6. The cumulative shape resembles a telescope, hence the name "telescopic deformation". The process accommodates tendril-like shapes, in

the sense that surfaces can recursively support branches off other earlier branches.

Figures 28a-c illustrate an example of the misfit reduction process. Suppose that we want to reduce the misfit in approximating a tendril shape by a plane, see Figure 28a. We subdivide the tendril using height field planes that approximately set to the tendril's critical points.

We have generated a sequence of truncated collars that reduce the misfit. We are not done, however, since this approximation is not differentiable at any point on a collar ring separating two truncated cones. We remedy this deficiency by replacing a thin swath about the ring with a thin swath about the equator of a sphere.

Figures 29a-c illustrates an example of blending a non-differentiable join of two collars. The idea is to map given instance (Figure 29a) to the one situation that we understand how to fix (Figure 29b). The one situation that we understand how to fix is an isosceles right triangle with an inscribed circle such that the center of the circle is the centroid of the triangle. We apply the linear transformation shown in Figure 29c to the isosceles right triangle in panel shown in Figure 29b to the exterior and interior triangles - corresponding to θ_1 and θ_2, respectively - in Figure 29a.

The misfit reduction procedure is as follows.

1. We construct height field contours on the noisy surface S. Remember that the height field is taken normal to the smooth shape approximation S*.

2. Working top down, we project each contour to S*. It is possible that the projection of successive contours cross.
3. We approximate each contour projection in two steps. First we locate all 1D critical points - minima, maxima, and inflection points. Second we fit a smooth approximation to each section of the projected contour; where a section is delimited by critical points.
4. We triangulate the interior of each projected contour, and then construct tetrahedra using consecutive contours.
5. We approximate the cap/cup corresponding to the innermost ring of the bull's eye with the ring's closure in the plane.

We next consider how to describe a branching structure of hills that separate a region into multiple valleys. Figure 30 shows as a geological example a water breach as indicated by the white arrow.

Here is a compact description of this branching structure.

1. Find the ridge edge in the branching structure. The ridge edge is a connected (therefore degenerate) set of critical points.
2. We assume that as typical cross section is a conic section, e.g., a parabola, an ellipse, etc.
3. We allow for stretching and contracting of the cross section. We call a region over which the typical cross section stretches or contracts a "transition zone". We provide linear interpolation between the start and stop position cross sections.

4. We anticipate a valley that runs perpendicularly to the ridge edge. For the case of a branching structure, we treat a valley of this type as a misfit. The following NASA aerial reconnaissance image contains active breaches in the ridge structure.

We consider a more challenging example. Figure 31 is a NASA Shuttle Mission photograph of the Richat Structure in Mauritania. NASA believes that most likely explanation of the origin of this structure is that it is uplifted rock sculpted by erosion. NASA also says that there is no widely accepted theory that explains why the Richat Structure is nearly circular.

The dominant shape in the Richat Structure is a nested sequence of toroidal structures. Because of erosion, some of the toroidal structures exist as sections of a torus only. Ecker argues on pg. 4-5 of his lecture notes that a torus satisfies mean curvature flow with respect to its mean curvature. This flow is singular, in the sense that in finite time the circular cross section shrinks to a point and hence the torus shrinks to a circle. This is a second example of the fact that mcf evolution need not preserve the dimension of a shape. (The other example is an uncapped cylinder whose radius r(t) is given by the formula $r(t)=\sqrt{r^2(0)-2t}$, *provided that* $t\in(0,\frac{r^2(0)}{2})$. In finite time the uncapped cylinder collapses to its axis of symmetry.

With respect to known techniques, Rouby et al. describe a parameterization algorithm for triangulated surfaces. See, D. Rouby, H. Xiao, J. Suppe, 3D Restoration of Completely Folded and Faulted Surfaces

Using Multiple Unfolding Mechanisms, AAPG Bulletin 84(6), June 2000, pg. 805-829. This method involves projecting the triangulation onto the (x,y) co-ordinate plane. It is not clear how to compensate for triangles that have a near singular projection. Also, the projection of multiple triangles onto a common plane can lead to a complicated overlapping and slivers. These are the sort of numerical instabilities that we want to avoid and which this algorithm does avoid.

A description will now be give for 3D conformal grid generation and reconstruction of shape from disconnected pieces, according to the invention.

Shape identification improves the performance of our incremental 3D conformal grid generator. Given a sub-volume V with boundary $\partial V = S$, we uniformly approximate S as a collection of trimmed ideal elementary shapes $\{E_m\}$. Then we enclose S in a tight sequence of rectangular prisms $\{P_k\}$ such that the "vertical" edges of the prism are normal to the ideal elementary shape approximants.

We generate a 3D conformal grid in 3 parts.

1. $\partial P_k \cap S$, which is the part between the prism faces and the measured surface S.
2. The bounding box B_m of each trimmed ideal elementary shape E_m.
3. A prism $P^* \subseteq V$ such that $P^* \cap B_m = 0$

We use a proportional spacing correlation scheme to grid part #1. In part #2 we use Em's parametric expression for normals to grid Bm. In part #3 we grid P* in the obvious way. The incremental nature of the

procedure follows from the subdivision of the grid into regions associated with the prismatic enclosure of S and the uniform approximation by trimmed ideal elementary shapes.

Figure 32 shows a conformal grid induced from a proportionally spaced correlation scheme. We use a proportional spacing correlation scheme to define the grid iso-surfaces. Here is an ideal application of this mechanism (This is an idealization of a cross section through the Gullfaks field.). We see that the sub-blocks have approximately the same z-direction thickness. It is irrelevant how the horizontal extents correspond. In other words, we can generate either a regular spacing grid or an irregular spacing grid. We remark that a compromise such as a "tartan grid" (also known as a rectilinear grid) is more memory efficient than a regular grid but still has a convenient algebraic lookup function.

We observe that a correlation scheme implements a cheap form of mean curvature flow and if generated independently of a parameterization, then the conformal grid is a roundabout way to also generate a parameterization.

We conclude this part of the description with a discussion of a way to convert an existing 3D Cartesian grid to a conformal grid. Figure 33 illustrates a non-conformal 3D Cartesian grid. As is well known, it is non-trivial to trim grid cells that cross volume boundaries. Here the background grid shown in dashed lines, crosses the overburden. It is clear in this diagram that the background grid cells do not conform to lithological boundaries.

We remedy these deficiencies in the following way.

1. We attach the volume of interest to a spatial frame.
2. We conformally grid the volume that lay between the overburden and the reservoir.
3. For best results we want a transition zone from a Cartesian grid to the conformal grid, preventing reverberation in the grid across lithological boundaries.

Forensic reconstruction will now be discusses. Suppose that an application identifies a set of disconnected 2D patches and would like to construct a surface from the patch set. We show how mean curvature flow enables us to construct such a surface - hence the sub-title for this discussion. This technique will be seen to be similar in execution to grid generation, which is why we discuss it here.

Suppose that we have a collection of 2D patches in R^3. We assume that all of the patches are oriented in a consistent manner, which must be the case if all of the patches are taken from a common surface. We construct the solution using patches or parts of patches that have a common Gaussian curvature signum. We do not insist that the Gaussian curvature signum be constant across the patch point set. However, if it is not constant, then we use only those patches and parts of patches that have the same signum to construct a surface. This procedure can create holes in the surface. We fill in these holes with the remainder of patches that were used only partially. Some patches with the opposite signum may not fill in holes, but instead form folds in the surface. We

construct a second surface from these patch point sets and union the two parts together.

We remark that the following algorithm is applicable to the task of sewing together parts of the bounding surface of a geobody, e.g., a salt body.

Our method is as follows.

1. We assume that the velocity of the flow equals 1, so that a time interval is equal to a distance.
2. For each patch or region of a patch R that has (+) signum Gaussian curvature, we define a uniformly expanding mean curvature flow with initial condition equal to R.
3. These patches are taken from a common surface, so we sample each flow at the same time step increments.
4. We stop a particular flow when it intersects another flow pattern.
5. Eventually each flow intersects a different flow.
6. It may be that the confluence of two flows is not differentiable. If this happens, then we define a flow to smooth the sharp angle. Alternatively, we can smooth the sharp angle using the Squeeze operator defined in the Misfit Reduction algorithm.

If a formation contains a tunnel, then we may wish to reverse the dissolution process, i.e., fill in the tunnel. In this situation we will approximate the tunnel as a collection of uncapped cylindrical and toroidal sections. Ecker's lecture notes show that mean curvature flow applied to an uncapped cylinder will shrink the 3D surface onto its 1D axis of symmetry in finite time. Smocyzk has obtained a comparable result for a torus. His result shows that a torus collapses under mean curvature

flow to its inner parabolic circle in finite time. We conclude that when applied to a tunnel, mean curvature flow will collapse the tunnel to a curve in finite time.

Figure 34 is an image of the Devil's Potholes, South Africa. We can identify two different kinds of pothole formations in this image. The circled pothole on the right is well described as a cylinder. We can collapse it to its axis of symmetry - which is a line - under mean curvature flow. The pothole on the left is more complex. The top of this region is a curved throat, which is followed by a sharp edged cone. Finally there is a toroidal section that is turning away from the viewer. We know that each section will collapse to a singular edge in a finite amount of time. Taking the longest time interval needed to collapse a section of this structure, we guarantee that the entire pothole will collapse to a polygonal path.

We now discuss a related problem. Given an image of a layered sequence, suppose that an unconformity. The unconformity will erase everything in the image that is above the unconformity. How good a reconstruction of the eroded interface can I achieve, given just the migrated image. As an example, we return to the diagram of a cross section of a shallow sequence in Turkmanistan shown in Figure 3. We are interested in the guess of what the missing section of the layer looks like.

Our algorithm assumes that the formation satisfies the following assumptions.

1. There exists a reference layer such that the visible part of the sequence is well approximated by a single reference surface adaptively sampled

correlation scheme. In the above schematic, the vertically striped layer R is the reference layer.

2. We reconstruct the eroded region of a layer by evolving the reference interface under mean curvature flow until the front joins the unconformity. In the above schematic, the reconstructed interfaces are shown as dotted outlines above the unconformity.

While it may not be obvious from Figure 3, conformal grid generation is a very short time solution to mean curvature flow. In other words, if erosion had not been imposed then we would recognize the conformal grid generation in the framework close to the reference surface and flattening further away. As an illustration, we consider Figure 35, which is a NASA LANDSAT image of the Yukon River delta (NASA Geomorphology plate D-9). We focus on the boundary cracks that subdivide the rounded joint at the left top of the image. These boundaries delimit curvature flow regions that collectively form the bend in the deltaic mass. It has been proposed to use a diffusive process. See, J. Davis, S. Marschner, M. Garr, M. Levoy, Filling holes in complex surfaces using volumetric diffusion, First International Symposium on 3D Data Processing, Visualization, and Transmission, Padua, Italy, June 19-21, 2002. This reference does not make use of curvature information in the algorithm used. Furthermore, the reference does not deal with closing 3D voids such as tunnel closure.

We have discussed how to construct a patchwork covering of an implicit surface from first order Taylor polynomials. The error term is quadratic with coefficients that are the principal curvatures defined at a point that is somewhere within the circle of convergence about the expansion point. The radius of the circle is chosen so that the error term is smaller than a user-defined tolerance. The error estimate is not sharp, because it is not obvious where to evaluate the error term's principal curvature values, i.e., what is the definition of α. Since this error estimate is not sharp, we supplement the Taylor representation with a fast technique to evaluate α.

From curvature analysis we derive a representation of a surface as a connected sum of trimmed elementary shape. Some examples of elementary shapes are (sections of) an ellipsoid, hyperboloid, cyclide, and a prism. An elementary shape has algebraic expressions for mean curvature and Gaussian curvature. These expressions can be substituted into the quadratic formula to generate an algebraic expression for principal curvature. Unfortunately the resulting expression is often so complex algebraically that a symbolic algebra package such as Mathematica® must be used for any manipulation other than simple evaluation. This is awkward in an Engineering environment, so a low order Taylor series approximation is preferable.

Here is an intersection algorithm for implicit surfaces. This algorithm assumes that every surface's signed distance function has been defined on a shared grid.

Notation

S_1 implicit surface #1

σ_1 a point on S_1

τ_1 parametric definition for σ_1

S_2 implicit surface #2

σ_2 a point on E_2

τ_2 parametric definition for σ_2.

G a shared 3D grid

C a grid cell in G such that $C \cap S1 \cap S2 \neq 0$

c_j a point in $C \cap S_1 \cap S_2$.

σ_{12} a point in $C \cap S_1 \cap S_2$.

Intersection algorithm

1. Find all grid cells $\{C_k\}$ that surface S_j intersects. A grid cell is involved if and only if the signed distance function is not constant at all grid cell corners.
2. In this algorithm we want to work with surface patches that project invertibly onto a face of grid cell. We subdivide the part of a surface contained in a grid cell into the desired patchwork by checking the surface normal field restricted to the grid cell. We place a point on the surface in a patch exactly when the unit normal at the point is within tolerance of being parallel to all other surface points that are already assigned to the patch.

For each S_1 patch find all S_2 patches such that their corresponding sdf patterns do not rule out intersection.

For clarity we assume that each surface contains exactly one such patch.

Loop$0:

3. Let c_0 be the midpoint of the line segment λ_0 connecting two faces of C such that the signum of the sdf for S_i on one of the connected faces is different from that on the other.
4. Let $j = 0$.

Loop$1:

5. Project c_j onto S_1 and S_2, respectively.
6. Label the projection s_{1j} and s_{2j}, respectively.
7. Either $s_{1j} = s_{2j}$ or not.
8. If $s_{1j} = s_{2j}$, then go to **Label$2**.
9. If $s_{1j} \neq s_{2j}$, then construct the line segment λ_{j+1} in C_k connecting s_{1j} to s_{2j}.
10. Let c_{j+1} be the midpoint of λ_{j+1}.
11. It might be the case that $c_j \approx c_{j+1}$. We expect to see this when a very thin hyperbolic neck is contained in the same cell as C_k.
12. If $c_j \approx c_{j+1}$, then we want to jump away from this hopeless local minimum. We do this by comparing the signum of the sdf for s_{1j} and the signum of the sdf for s_{2j} to signum of sdf obtained on the grid cell faces joined by the line segment λ_0. Moving in the direction that differs from the current values, jump to the midpoint along λ_0.
13. Increment j and return to **Loop$1**.

Label$2:

We use a Newton algorithm to find another point of intersection.

Loop$3:

14. Let (x_{12}, y_{12}) be a point of intersection for S_1 and S_2 in C and suppose that (x_{12}^*, y_{12}^*) is another point of intersection in C. Expanding each surface in a 1st order Taylor series about (x_{12}, y_{12}), we have

$$S_1(x_{12}^*, y_{12}^*) = S_1(x_{12}, y_{12}) + \nabla S_1(x_{12}, y_{12}) \cdot (x_{12} - x_{12}^*, y_{12} - y_{12}^*)$$
$$S_2(x_{12}^*, y_{12}^*) = S_2(x_{12}, y_{12}) + \nabla S_2(x_{12}, y_{12}) \cdot (x_{12} - x_{12}^*, y_{12} - y_{12}^*)$$

15. Subtracting, we have 2 linear equations in two unknowns. Solve for the non-trivial solution

$$0 = \nabla (S_2 - S_1)(x_{12}, y_{12}) \cdot (x_{12} - x_{12}^*, y_{12} - y_{12}^*)$$

16. Return to **Loop$3** until (x_{12}^*, y_{12}^*) is acceptably close to being another point of intersection in C.
17. We compute the intersection curve between (x_{12}, y_{12}) and (x_{12}^*, y_{12}^*) by repeating the midpoint subdivision algorithm in **Loop$2**.
18. Return to **Loop$3** and repeat the 1st order Taylor series algorithm in Loop$2 on both ends (x_{12}, y_{12}) and (x_{12}^*, y_{12}^*) until the curve crosses the faces of C_k.
19. Return to **Loop$3**and continue processing grid cells in $\{C_k\}$ until exhaustion.

Visualization of an intersection curve is as follows.

1. Project the intersection curve onto the internal cylindrical parameter space.
2. Facet the cylinder using a constrained Delaunay algorithm.

3. Invert the mapping, projecting the triangulation of the region enclosing the "flattened" intersection curve to the parent implicit surface.

We have described a curvature-adaptive method for placing sample points on a surface and generating a narrow band octree from them. Now we discuss how spatial frames can be used to implement an efficient update mechanism. For details of the reappearance of SIGMA's hybrid grid-mesh concept, refer to U.S. Patent Application Serial No. 09/163,075, incorporated herein by reference.

Each geological feature has its own octree which overlays part of the background octree. An overlay can cover a strictly smaller region of the background, and this small region can be sampled differently (adaptively) from the background. The sampling can be adapted to the complexity of the framework region that the overlay encloses. The overlay changes as the framework region changes. A separate spatial frame is assigned to control each octree overlay. Overlays are loaded on demand. Within a spatial frame the sampling can be adjusted in an adaptive manner. A frame boundary sample node can be part of multiple octree overlay. An entity that is outside a particular spatial frame learns about the frame's enclosed shape by interrogating the enclosing spatial frame. Given an octree identifier and a location inside or on the boundary of the octree's enclosing frame, the local cpt returns the cpt and sdf for the remote octree overlay. Adjacent frames might support a different set of and number of framework surfaces.

Given a region of interest, we associate to each spatial frame the point set that the frame contains. We

represent the set of spatial frames associated with a region of interest as a directed acyclic graph. Two parent frames that partially overlap will be represented in the graph as nodes that point to a common descendant. Thus spatial frames constitute a topology graph.

As an example, a vsp was acquired over part of the Zechstein Salt formation. Figures 36a and 36b show, for reference, the background Zechstein Salt and the region in the Zechstein where the vsp was acquired. Figure 37 show the frame graph that ties the vsp region of interest to the Zechstein Salt background. We use the inner frame to outer frame relationship to express "A is a boundary of B" and "A is logically part of B". In GQI terminology a spatial frame as defined herein is equivalent to a gqi_Frame_t. We have extended this functionality two ways. First, we maintain logical containment, i.e., feature relationships. Second, we allow mixing space and time frames.

Spatial frames are useful in subdividing a faulted region to match regions subject to different physics. For example, Figures 38a, 38b, 39a and 39b illustrate the separation of faulted sediments from unfaulted sediments. Figure 38a and 38b show the case of a sequence of sediments such that some but not all of the sediments have been faulted, and a simple normal fault is involved. Figures 39a and 39b show the case of a fault network where some of the faults in the network emanate from other faults. Figure 39b shows that the unique final configuration of spatial frames that partition the volumes shown in Figure 39a. Using mathematical induction on the number of faults in a compact region of interest, we conclude that it is immaterial in what order

spatial frames are assigned to isolate distinct sedimentary regions. In other words, the final subdivision is always the same no matter what the order of isolation is.

We think of mean curvature flow as an evolutionary process. For simplicity, we assume that any evolutionary process is a structure group of diffeomorphisms of some 4D fibre bundle. All information regarding the process at a moment in time is encoded in a time frame. A time frame contains a reference to a region of interest that in turn is represented as a 3D fibre bundle. We do not demand that an evolutionary process provide a physically plausible explanation of a formation state, rather it is enough if the visual expression appears plausible.

Figure 40 illustrates a time-lapse seismic evolution (steam injection front tracking, with the left panel "before" and the right panel "after".). We discuss now how we use spatial frames to define a topology graph. Let S be an implicit surface and let $\{E_k\}$ be a family of elementary shapes that approximate S. Each E_k reduces its misfit with S by fitting a disjoint region of S to a telescopic extrusion of E_k.

We use a different spatial frame to contain each telescopic extrusion and attach the collection of these frames. We assign each elementary shape to its own spatial frame and refer to the misfit reduction through attachment of the spatial frame list to the parent elementary shape frame. Figure 41 shows the reference structure for this set of relationships.

We summarize the contents of the new class instances that we have defined in this paper.

Spatial frame class

1. Database identifier.
2. The parent spatial frame.
3. The list of children spatial frames.
4. A static hash table that provides the address of a spatial frame given a database identifier.
5. The outermost grid cell boundary, given as a pair of synchronized lists.
   a. The first list is a set of IJK base grid cells. The second list is in 1-1 correspondence with the first list.
   b. The second list is an ordered list of {left/right, up/down...} steps that define the grid cell face sequence that form the boundary.
6. The boundary curve contents of the grid cell boundary.
   a. Mandatory is a list of minima, maxima, and inflection points, ordered by arc length coordinate from the first critical point in this list.
   b. Optional is a list of conic sections that approximate the shape of the boundary restricted to each consecutive pair of critical points.
7. Transition zone, given as a grid cell thickness surrounding the interior of the outermost boundary. Zero thickness is acceptable.
8. The list of data base identifiers used to define the surfaces that intersect this spatial frame.
9. The data base identifier of the octree attached to this spatial frame.
10. Shape contents enclosed by the outer boundary. This can be void when the frame defines a hole..
11. Methods
    a. Put/GetNeighbor

b. Put/GetLogicalNeighbor
c. Put/GetShapeContents
d. Put/GetSurfaceContents
e. ReseampleSurface
f. Put/GetOuterBoundary
g. Put/GetInnerSpatialFrameList
h. Put/GetParentSpatialFrame
i. Put/GetTemporalFrame

12. Evolutionary law
a. Parameter list
b. Boundary conditions
c. Initial conditions
d. Status

Shape index manifold

1. Database identifier
2. Status
3. Floating point references
a. XYZ
b. ABC
4. Misfit threshold
5. Shape index charts
6. Boundary representation node

Shape index chart

1. Database identifier
2. Symmetry group isomorphism class
{Sphere, Cylinder, Cone, Frustum, Torus, Ellipsoid, Hyperboloid_Type_I, Hyperboloid_Type_II, Circle, Ellipse, Cube, Tetrahedron, Square, Triangle, Rectangle, Cyclide, Trivial}
3. Parameter vector ABC
4. Canonical position transformation [Rotation matrix and translation vector]

5. Shape index manifold
6. Shape index interval
7. Critical point list
8. (Static) analytical methods
    a. Evaluator
    b. Normal
    c. Tangent
    d. First Fundamental Form
    e. Christoffel symbols
    f. Second Fundamental Form
    g. Gaussian curvature
    h. Mean curvature
    i. Principal curvature
    j. Shape index
    k. Signed distance function
    l. Closest point transform
    m. Parameter estimation
    n. Extrude
    o. Offset
    p. Adaptive sampling
9. Standard methods
    a. Sve
    b. Restore
    c. I/O compress
    d. I/O decompress
    e. Delete
    f. Copy
    g. Newa
10. Misfit reduction
    a. Absolute amount
    b. Relative amount
    c. Base type
        {Ellipse, Circle, Square, Triangle, Rectangle}
    d. Parameter vector list
        {u, v, normal offset}

1D Boundary

1. Conic section class
   {Ellipse, Circle, Line, Parabola, Hyperbola
2. Plus side
   a. Shape index chart
   b. UV start stop
3. Minus side
   a. Shape index chart
   b. UV start stop
4. Boundary representation node

Critical point assertion

(We specify two lists, separating min/max from saddle point.)

1. Shape index chart
2. UV location
3. Chart symmetry

We use Dustin Lister's trick of using a 2s complement 16-bit integer to subdivide length scale field data into (+/-) 32K increments. Given a reservoir model of size 9 square miles by 50000 feet, we can resolve data to 1 cm. Applying Dustin's idea to Shape index charts and dependent lists, we obtain a surprisingly compact data structure. For example, suppose that a shape index manifold contains 48 charts such that each chart supports 48 misfit reduction "boxes". Further, suppose that each chart contains 4 critical point orbits relative to the chart symmetry group. Then the Shape Index manifold will consume on the order of 34000 bytes ≈ 33 Kbytes of memory. These choices are arbitrary, but far exceed the empirically estimated values for the Top of Salt surface in the November 2002 Implicit Surface Proof of Concept

data set. In that demonstration, this surface consumed slightly more than 1 MByte of memory, which implies that curvature-based methods are naturally 30 times more conservative in memory utilization.

Quadratic Taylor expansion disk class

1. Status {CRITICAL_POINT_EXPANSION}
2. Expansion point
3. Principal curvatures
4. Rotation matrix and translation vector
5. Error tolerance
6. Shape index interval
7. Trimming curve discrete samples list

Characteristic length scale cone class

1. Equivalence class
2. Status
3. Length scale
4. Top
   a. Radius
   b. Center
   c. Percent error
5. Bottom
   a. Radius
   b. Center
   c. Percent error
6. Slant height ratio

An example of applying the techniques described above to a relatively complicated surface will now be discussed. The example used herein is a synthetic surface designed to be an "unfriendly" test case.

Approximately 14500 triangles were created from 7349 vertices. The representation requires approximately 1Mb of memory.

Note that discrete estimators for Gaussian and mean curvature were used to compute the shape index. See, M. Desbrun, M. Meyer, P. Schroeder, A. Barr, Discrete Differential-Geometry Operators in nD, Technical Report Caltech, 2000. For example, the discrete estimator for mean curvature H*(P) evaluated at a point P is

$$H^*(P) = \frac{1}{4^* area} \sum_i (\cot\alpha_i - \cot\beta_i) \cdot (P - Q_i)$$

Figure 42 is a schematic illustration of the definition of the variables in the mean curvature estimator. See, G. Stylianou, Comparison of triangulated surface smoothing algorithms, http://3dk.asu.edu/archives/seminars/presentation/Compsmthal.ppt.

The discrete Gaussian curvature estimator K*(P) evaluated at a point P is given by

$$K^*(P) = 2\pi - \sum_i \theta_i(P),$$

where θ_i is the i^{th} triangle's angle in the star of P rooted to P.

Figure 43 is an image of the co-triangulated irregularly spaced mesh that represents the present example of the top of the salt.

Several smoothing methods for triangulated surfaces have been considered, but all of them assume a regular spaced carrier grid. See, A. Hubeli, Multiresolution Techniques for Non-Manifolds, Diss ETH No. 14625, Computer Graphics Laboratory, Department of Computer

Science, ETH Zurich, 2002. This surface is sampled irregularly, the mesh surface is re-samples by interpolating missing sample points. Figure 44 shows the surface when re-sampled by interpolating missing sample points. The surface of Figure 44 has approximately 10000 points versus 7900 points in the original mesh shown in Figure 43.

The surface of Figure 44 is noisy everywhere, but the noise is low amplitude. The preferred smoothing software according to A. Hubeli, Multiresolution Techniques for Non-Manifolds, Diss ETH No. 14625, Computer Graphics Laboratory, Department of Computer Science, ETH Zurich, 2002, incorporated herein by reference. The smoothing software moves points in the horizontal plane to minimize curvature, so it is necessary to project one version of the surface onto another when different numbers of iterations are applied

Figure 45 shows the re-sampled surface after 25 iterations of smoothing. This surface is significantly smoother, but after comparing the two images we concluded that we have not sacrificed its intrinsic low frequency contents. The mean curvature flow preferentially removes high frequency noise and leaves intact low frequency intrinsic shape.

Figure 46 shows the shape index map for the re-sampled triangulated surface after 25 iterations. There are regions of approximately the same shape index that contain islands that have significantly different shape index. An example of this behavior is the red body in the bottom middle that contains two blue bodies.

We consider the following labeling options for this image. We recall that "label" is a grid cell equivalence class identifier.

1. Label each blue body and the surrounding red body as separate shapes.
2. Label the two blue bodies as part of the same shape and consider the blue shape to be distinct from the enclosing red shape.
3. Label the red body as blue body misfits.
4. Label the blue bodies as red body misfits.

Figure 47 shows that there are 33 shapes in the example. According to the data structure definition described above, about 512 bytes of storage are needed to express a shape with zero misfit reduction. Assuming adequate misfit reduction per shape consumes another 512 bytes, we conclude that we can well approximate this noisy surface in 33 Kbytes of data structure. We need about 1 Mbytes of storage to define this surface, so we obtain a 1000 / 33 ≈ 30-fold compression.

It is important to understand that we do not equate a geometrical label to a geological theory. We prefer a description of the topography that uses the least number of parameters.

According to preferred embodiments of the invention an important implicit surface data structure is the narrow band octree. The curvature analytical enhancements to implicit surface technology described herein enable the construction a reservoir framework using significantly less memory and CPU than conventional triangulated surface technology requires. Additionally,

the curvature-based methods describe herein enable the construction of a new generation of structural framework. We enumerate a number of advantages of curvature analysis in support of implicit surface methods, according to preferred embodiments of the present invention.

I. Computer resource economy

a. We describe the shape of a geological surface in terms of explicit surface forms, e.g., ellipsoid and torus, rather than contextually in terms of a technology used to represent shape, e.g., triangles.

b. We replace numerical computation of curvature, normals, signed distance functions, etc. by analytical formulae which enables us to drop the buffering needed to hold the sampled data.

II. Surface flattening

c. Many operations on surfaces are easier to perform when a flattened version of a surface is available.

d. We refer to the flattening as the "parameterization" of the surface.

e. When we construct the parameterization of a surface, then we also generate an estimate of the geometric strain needed to flatten the surface. Strain says how comparable is the flattened version to the given surface.

f. Parameterization is much more useful if the flattened surface can be placed in the framework, rather than on some planar surface that is outside the framework. Shape analysis enables us to embed the parameter space surface in our xyz coordinate space.

III. 3D conformal grid generation and forensic reconstruction

g. Using surface parameterisation, shape analysis knows how extract a 3D conformal grid from each framework sub-volume.

h. Regular grids are convenient for simulation. That does not mean that we have to permanently record a regular sampling in regions that show little or no variation. We equate this variation to an estimate of curvature. On demand we provide regularly spaced samples in low curvature regions.

i. We call this curvature-adaptive sampling. Curvature adaptive sampling does not waste space on recording redundant information.

j. Curvature-dependent adaptive grid generation is more economical than the non-curvature-adaptive form. An application can easily extract a perfectly uniform 3D grid on demand.

k. Mean curvature flow can be used to fill in holes and to construct a plausible representation of an eroded region of a sequence.

IV. Framework construction, editing, and reconstruction

l. Based on the implicit surface's signed distance function, we construct a connected sum of shapes that are sectors of a conic section fibre bundle.

m. Boolean operations that take shape into account are more efficient than those that do not.

n. Sending and receiving elementary shape descriptions is inherently more efficient than sending and receiving the corresponding triangulation. The Marching Cubes algorithm can be used to triangulate an implicit surface's elementary shape constituents.

o. The identification of elementary shapes is based on application of mean curvature flow (mcf).

p. We do not worry if a process is well approximated by mcf. Rather all that matters is whether the elements in a framework can be defined as the solution to a flow problem.

q. We use structure synopsis diagrams to send and receive a high level resume of the connectivity and shape of a structural framework. This data structure extends the traditional Reeb graph summary of connectivity to a shape description that is intuitive - which is something a byte stream describing millions of triangles can never hope to achieve.

V. Noise suppression

r. Elementary shape identification can be applied to a noisy surface.

s. Shape analysis provides a tool to distinguish noise suppression from shape decay.

VI. Robust shape identification

t. Suppose that an implicit surface is represented in a 3D grid with a tri-linear interpolation function. We have discovered necessary conditions on the interpolation function coefficients in order that a grid cell in the grid contain a critical point. It is very easy and fast to test these conditions, so we can quickly locate a surface's critical points in the grid.

u. Group theory yields a robust classification of symmetry induced from the tri-linear interpolation approximation of the implicit surface's signed distance function. This is used to identify the optimal elementary shape

candidate shape that fits a single grid cell of the 3D grid representation of the implicit surface.

v. It enables local quantitative comparison of two surface shapes. The process identifies regions on the measured surface where there is poor agreement and provides an estimate of the energy expended in the geometrical transformation needed to finish the package.

Figure 48 is a schematic illustration of a system for improved extraction of hydrocarbons from the earth, according a preferred embodiment of the invention. Seismic sources 150, 152, and 154 are depicted which impart vibrations into the earth at its surface 166. The vibrations imparted onto the surface 166 travel through the earth; this is schematically depicted in Figure 7 as arrows 170. The vibrations reflect off of certain subterranean surfaces, here depicted as surface 162 and surface 164, and eventually reach and are detected by receivers 156, 158, and 151.

Each of the receivers 156, 158, and 151 convert the vibrations into electrical signals and transmit these signals to a central recording unit 170, usually located at the local field site. The central recording unit 170 typically has data processing capability such that it can perform a cross-correlation with the source signal thereby producing a signal having the recorded vibrations compressed into relatively narrow wavelets or pulses. In addition, central recording units may provide other processing which may be desirable for a particular application. Once the central processing unit 170 performs the correlation and other desired processing, it

communicates the seismic data to data processor 180 which is typically located at the local field site. The data transfer from the central recording unit 170 in Figure 7 is depicted as arrow 176 to a data processor 180. Data processor 180 can be used to perform processing as described in steps 300 to 316 in Figure 50 and 330 to 340 in Figure 51, as is described more fully below.

The seismic data collected from recording unit 170 which is usually a relatively large data set. Importantly, according to the invention, the data processing to generate an efficient and robust subdivision of shapes representing the seismic data is performed on data processor 180. In this way a compressed, stable, accurate representation of new data is transmitted to other processing centers.

At the field site, a subset 182 of a larger earth model 192 is provided to aid in the field activities. The after the subdivision of shapes, the Fragment earth model 182 can be updated with the newly acquired data for use locally.

Data processing center 190 is located away from the wellsite or field site, typically at an asset management location. In some cases data processing center 190 is physically distributed across a number of separate processing centers over a wide geographic region. Data processing center 190 integrates the subdivision of shapes representing the earth structures into existing earth model 192. The integration of both the geometry framework and material field properties is preformed. While in some cases the integration of the new shape information can be done at the field site, this is not normally done due to a number of factors including (1)

lack of full data set of earth model at the field site, lack of computational facilities, and lack of sufficient local expertise.

Once the earth model 192 is updated with the newly acquired information, updated earth model data from model 192 is preferably sent back to the field site data processor 180. The information sent back to the field site preferably includes both (1) shape information to update geometry framework and material field properties of earth model fragment 182, and (2) decisions relevant to field site activities based in part on the updated earth model 192.

For example, according to one embodiment, based on new information integrated in earth model 192 at data processing center 190, improved predictions of fluid flow are made though the earth structures. Based on these improved predictions the rate of extraction from production well 114 is preferably altered using surface equipment 116 to optimize production rates from reservoir rock 120 while minimizing likelihood of undesirable events such as water breakthrough.

According to an embodiment during the wellbore construction, based on new information integrated in earth model 192 at data processing center 190, improved predictions on the likelihood of structural failure of a wellbore 110 being drilled into reservoir rock 120 from drilling rig 112. Based on these improved predictions, the drilling plan used to drill the well 110 is preferably updated, for example to reduce the risk of wellbore stability problems, to steer the drilling activity more precisely to certain locations within the reservoir rock and/or avoid faults, etc.

According to another embodiment of the invention, data processing center 190 can more easily communicate geologic information from one earth model based on geometrical representation to another earth model based on a different geometrical representation. In this way, the invention can be used to facilitate communication of earth model information between different models. Similarly, according to another embodiment of the invention, the techniques described her used to facilitate the aggregation of geologic information from a number of geometrical representations of the earth structures.

Figure 49 shows further detail of data processor 180, according to preferred embodiments of the invention. Data processor 180 preferably consists of one or more central processing units 350, main memory 352, communications or I/O modules 354, graphics devices 356, a floating point accelerator 358, and mass storage such as tapes and discs 351.

Figure 50 shows steps in a method for processing data used for hydrocarbon extraction from the earth, according to preferred embodiments of the invention. In step 300, sampled data representing earth structures is received. In step 310 one more symmetry transformation groups are identified from the sampled data. In step 312, a set of Morse theoretical height field critical points are identified from the sampled data. In step 314, a plurality of subdivisions of shapes are generated such that when aggregated, the subdivisions accurately, efficiently, and robustly represent the original earth structures. The generation in step 314 is based on the set of identified critical points and the symmetry transformation groups, according to the techniques

descried above and in further detail in Figure 51. In Step 316, earth model data is processed using the generated subdivision of shapes. In step 318 activity relating to extraction of hydrocarbons from a hydrocarbon reservoir is altered based on the processed earth model data. Various embodiments involving processing of earth model data and altering activity in steps 316 and 318 are described above with respect to Figure 48.

Figure 51 shows further detail of steps in generating an efficient and robust subdivision of shapes, according to preferred embodiments of the invention. In step 330, each of the identified symmetry transformation groups is preferably associated with to a plurality of shape families. Each of the shape families preferably includes a set of predicted critical points. The shape families for each symmetry transformation group are preferably contained in a lookup table. In step 332 a shape family is selected from the plurality of shape families. The selection is preferably based on closeness of correspondence, or best fit, between the identified critical points from the original sampled data and the predicted critical points of the selected shape family.

Note that each of the symmetry transformation groups is preferably a set of diffeomorphisms that act on a topologically closed and bounded region in space-time such that under transformation the region occupies the same points in space.

Each shape family preferably has an associated set of symmetry transformation group orbits, each orbit being associated with orbit information that specifies whether the orbit contains a predicted critical point and value of the Gaussian curvature of a point in the orbit. In

step 334, the orbit information from the set of symmetry transformation group orbits associated with the selected shape family is preferably applied to the original sampled data. In step 336 the result of step 334 yields a unique specification of a shape from the selected shape family. In step 338, each of the plurality of subdivisions of shapes is preferably generated by identifying a part of the uniquely specified shape that corresponds to the sampled data. In step 340, the identified parts are assembled, or sewn together, such that a representation of the earth structures is generated.

The assembled subdivisions are advantageously more efficient and robust than conventional methods. For example the number of parameters in each subdivision times the number of subdivisions is substantially less then would be needed using a faceted representation method, and the plurality of subdivisions is more numerically stable than third order or higher representation.

While the invention has been described in conjunction with the exemplary embodiments described above, many equivalent modifications and variations will be apparent to those skilled in the art when given this disclosure. Accordingly, the exemplary embodiments of the invention set forth above are considered to be illustrative and not limiting. Various changes to the described embodiments may be made without departing from the spirit and scope of the invention.

CLAIMS

1. A method for processing data used for hydrocarbon extraction from the earth comprising the steps of:

receiving sampled data representing earth structures;

identifying one or more symmetry transformation groups from the sampled data;

identifying a set of critical points from the sampled data;

generating a plurality of subdivisions of shapes the subdivisions together representing the earth structures, the generation being based at least in part on the set of identified critical points and the symmetry transformation groups; and

processing earth model data using the generated subdivision of shapes.

2. A method according to claim 1 wherein the identified symmetry transformation group is a set of diffeomorphisms that act on a topologically closed and bounded region in space-time such that under transformation said region occupies the same points in space.

3. A method according to claim 1 wherein each of the identified symmetry transformation groups corresponds to a plurality of shape families.

4. A method according to claim 3 wherein each of the plurality of shape families comprises a set of predicted critical points.

5. A method according to claim 4 wherein the step of generating subdivisions comprises selecting a shape family from the plurality of shape families that corresponds to the identified symmetry transformation group, said selecting being based on closeness of correspondence between the identified critical points from the sampled data and the predicted critical points of the selected shape family.

6. A method according to claim 5 wherein each shape family has an associated set of symmetry transformation group orbits, some of the orbits being associated with critical points and other orbits being associated with distinguished Gaussian curvature values.

7. A method according to claim 6 wherein each symmetry transformation group orbit of the selected shape family is associated with orbit information that specifies whether the orbit contains a predicted critical point and value of the Gaussian curvature of a point in the orbit.

8. A method according to claim 7 wherein the orbit information from the set of symmetry transformation group orbits associated with the selected shape family is applied to the sampled data thereby generating a unique specification of a shape from the selected shape family.

9. A method according to claim 8 wherein each of the plurality of subdivisions of shapes is generated by identifying a part of the uniquely specified shape that corresponds to the sampled data.

10. A method according to claim 9 wherein the identified parts of the uniquely specified shapes are assembled, thereby generating a representation of the earth structures.

11. A method according to claim 10 wherein the generated representation is continuous.

12. A method according to claim 11 wherein the generated representation is smooth.

13. A method according to claim 9 wherein the uniquely specified shapes are specified using differentiable functions including one or more of the following types: surfaces derived from conic sections, splines, general polynomials and trigonometric functions.

14. A method according to claim 1 wherein the sampled data is smoothed prior to said steps of identifying critical points and identifying one or more symmetry transformation groups.

15. A method according to claim 1 wherein the identified critical points are Morse theoretical height field critical points consisting of the following three types: minima, maxima and saddle points.

16. A method according to claim 15 wherein said step of generating a plurality of subdivisions comprises applying a canonical homogeneous transform such that the number of parameters needed to uniquely describe a shape in the earth structure is minimized.

17. A method according to claim 1 wherein the earth model data is geologic data, geophysical data, petrophysical data, mechanical earth model data and/or reservoir fluid flow data.

18. A method according to claim 1 wherein earth model data is processed such that earth models are updated, alternative versions of existing earth models are created, time-lapse earth models are generated and/or the earth model data is distributed to other earth models or other applications.

19. A method according to claim 1 wherein the sampled data represents sampled physical structure and material properties of the earth structures.

20. A method according to claim 1 wherein said step of processing earth model data comprises making predictions of fluid flow though at least some of the earth structures and wherein the altered activity is altering the rate of extraction based on said predictions.

21. A method according to claim 1 wherein said step of processing earth model data comprises predicting the likelihood of structural failure of a wellbore though at

least some of the earth structures and wherein the altered activity is altering the drilling of the wellbore based on the predicted likelihood of failure.

22. A method according to claim 1 wherein said step of processing earth model data comprises communicating geologic information relating to at least some of the earth structures between a first geometrical representation and a second geometrical representation of the earth structures.

23. A method according to claim 1 wherein said step of processing earth model data comprises aggregating information from a plurality of geometrical representations of the earth structures and wherein the altered activity is based at least in part on the aggregated information.

24. A method according to claim 1 wherein said step of processing earth model data comprises constructing an earth model to a user specified error tolerance using the generated subdivision of shapes.

25. A method according to claim 1 wherein each of the plurality of subdivisions of shapes is generated by identifying a part of a uniquely specified shape that corresponds to the sampled data.

26. A method according to claim 1 wherein the step of generating a plurality of subdivisions comprises the steps of:

analyzing curvature of the sampled data thereby generating a shape index field; and

identifying functions that fit the shape index field.

27. A method according to claim 26 wherein the functions are differentiable.

28. A method according to claim 1 wherein the plurality of subdivisions are generated such that the number of parameters in each subdivision times the number of subdivisions is substantially less than would be needed using a faceted representation method.

29. A method according to claim 1 wherein the plurality of subdivisions are generated such that they are more numerically stable than third order or higher representation.

30. A method according to claim 1 wherein the sampled data is a faceted representation of the earth structures.

31. A method according to claim 30 wherein the faceted representation is a triangle mesh.

32. A method according to claim 30 wherein the faceted representation is a grid.

33. A method according to claim 1 wherein the sampled data is data measured with seismic acquisition equipment.

34. A method according to claim 33 wherein said steps of receiving, identifying one or more symmetry transformation groups, identifying a set of critical

points and generating a plurality of subdivisions of shapes are preformed at or near the location where the sample data is measured.

35. A method according to claim 34 wherein said step of processing earth model data is performed in one or more locations remote from the location where the sample data is measured.

36. A system for improved extraction of hydrocarbons from the earth comprising:

a storage system adapted to receive and store sampled data representing earth structures;

a processing system adapted to identify one or more symmetry transformation groups from the sampled data, identify a set of critical points from the sampled data, and generate a plurality of subdivisions of shapes the subdivisions together representing the earth structures, the generation being based at least in part on the set of identified critical points and the symmetry transformation groups;

an earth model processing system adapted to processes earth model data using said generated subdivision of shapes; and

an interface to output the processed earth model data to an operator.

37. A system according to claim 36 wherein the identified symmetry transformation group is a set of diffeomorphisms that act on a topologically closed and bounded region in space-time such that under

transformation said region occupies the same points in space.

38. A system according to claim 36 wherein each of the identified symmetry transformation groups corresponds to a plurality of shape families, each of which comprises a set of predicted critical points.

39. A system according to claim 38 wherein the subdivisions are generated such that a shape family is selected from the plurality of shape families that corresponds to the identified symmetry transformation group, said selecting being based on closeness of correspondence between the identified critical points from the sampled data and the predicted critical points of the selected shape family.

40. A system according to claim 39 wherein each shape family has an associated set of symmetry transformation group orbits, each orbit being associated with orbit information that specifies whether the orbit contains a predicted critical point and value of the Gaussian curvature of a point in the orbit, and wherein the orbit information from the set of symmetry transformation group orbits associated with the selected shape family is applied to the sampled data thereby generating a unique specification of a shape from the selected shape family.

41. A system according to claim 40 wherein each of the plurality of subdivisions of shapes is generated by identifying a part of the uniquely specified shape that

corresponds to the sampled data, and wherein the identified parts are assembled, thereby generating a representation of the earth structures.

42. A system according to claim 36 as part of a system adapted to assist a decision making process relating to extraction of hydrocarbons from a hydrocarbon reservoir modeled by the processed earth model data.

43. A system according to claim 36 wherein the plurality of subdivisions are generated such that they are more numerically stable than third order or higher representation.

44. A system according to claim 36 wherein the sample data are acquired from the earth structures using seismic acquisition equipment, the storage system and the processing system are located at or near the location where the sample data are acquired, and the earth model processing system is located in one or more locations remote from the location where the sample data is acquired.

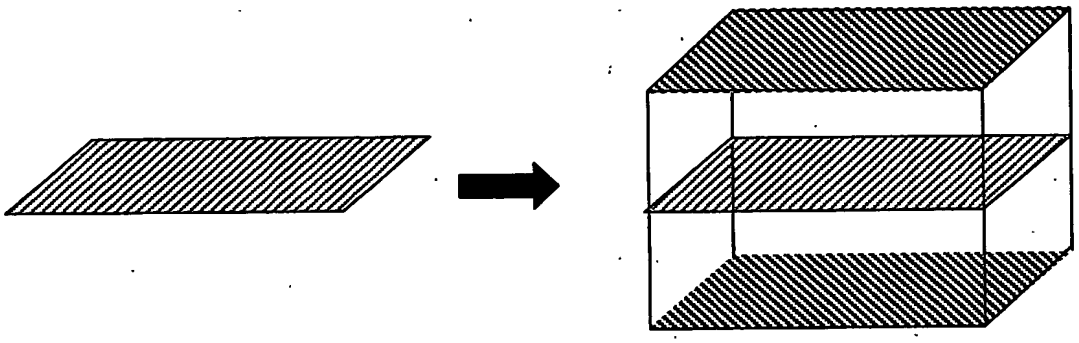

Figure 1

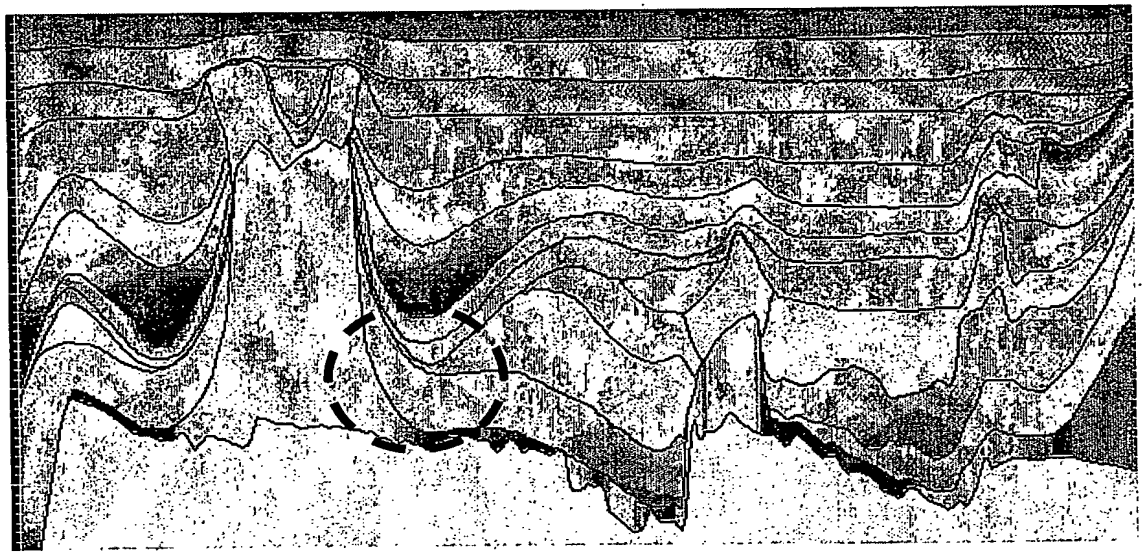

Figure 2

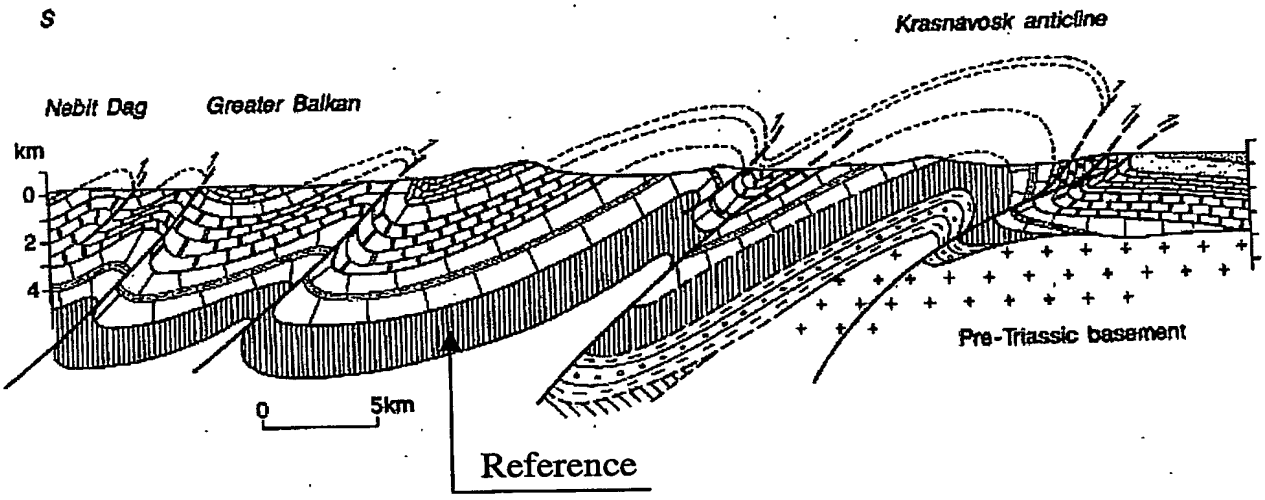

Figure 3

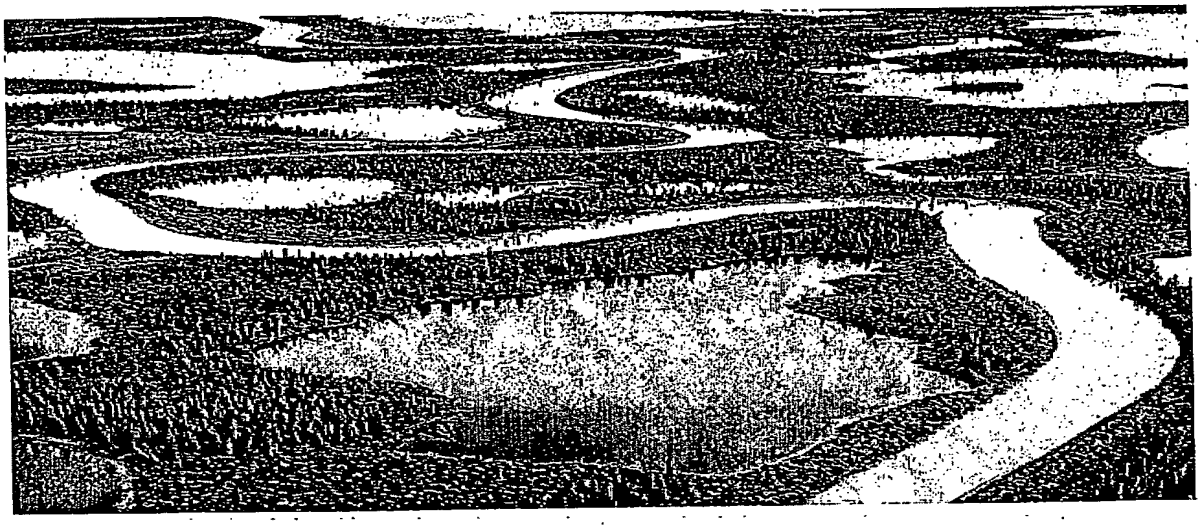

Figure 4

Y_{00}

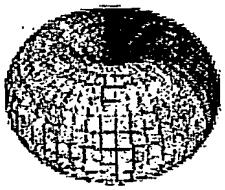

Y_{01}

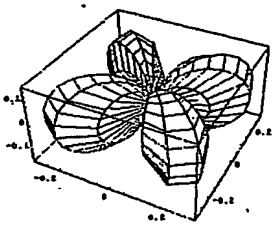

$Re(Y_{21})$

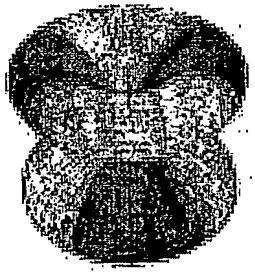

Im(Y32)

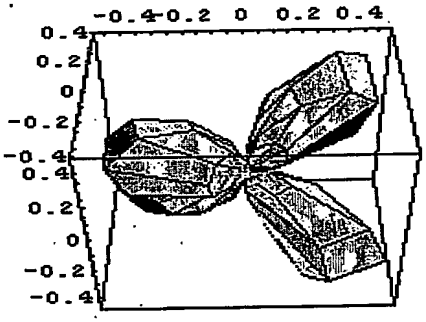

$Re(Y_{22})$

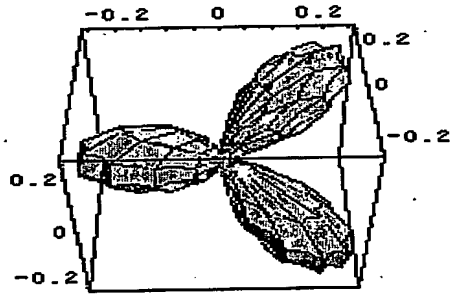

Y01 + Im(Y32)

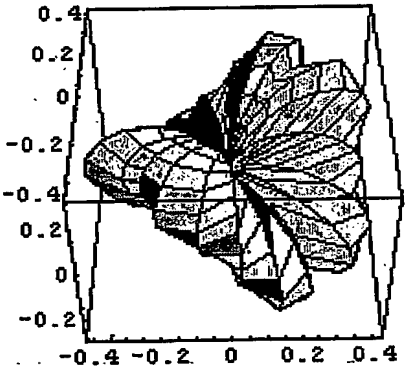

$Re(Y_{22}) + Im(Y_{32})$

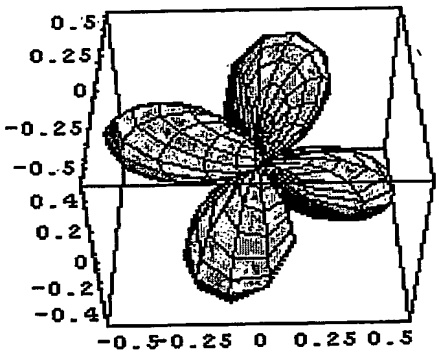

$Re(Y_{21}) + Im(Y_{21}) + Re(Y_{22})$

Figure 5

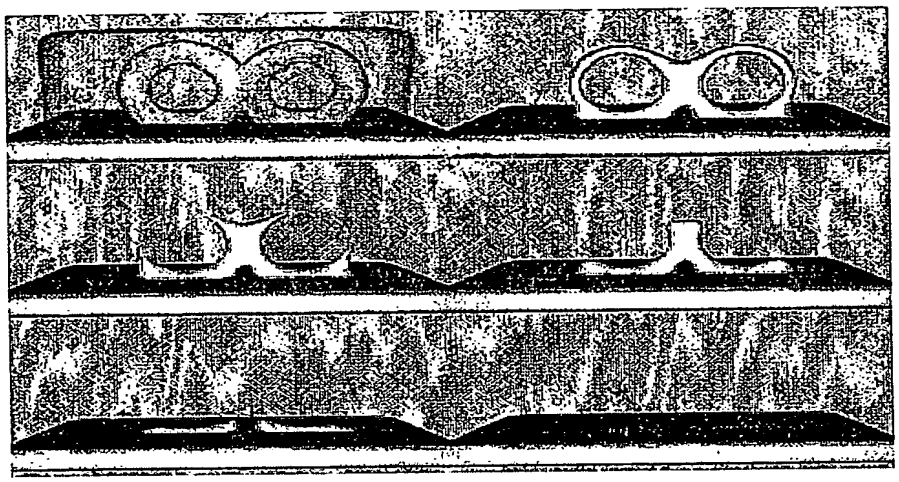

Figure 6

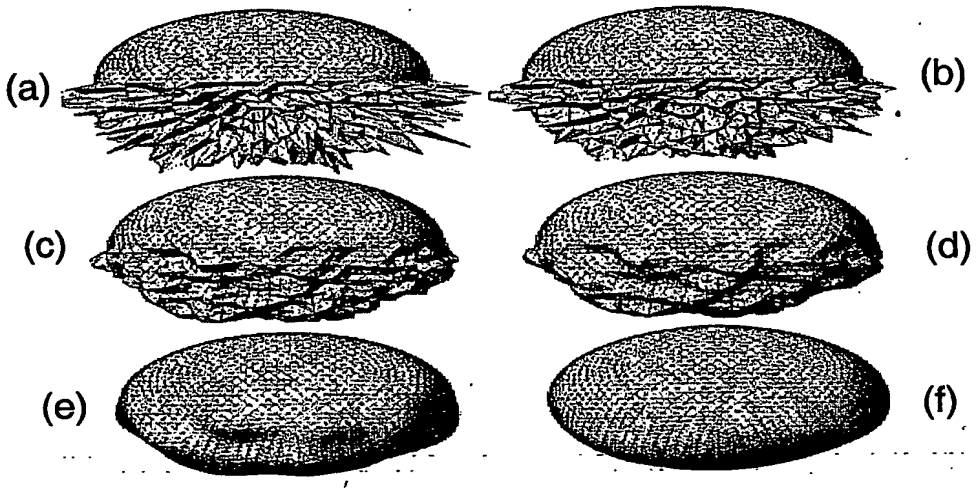

Figure 7

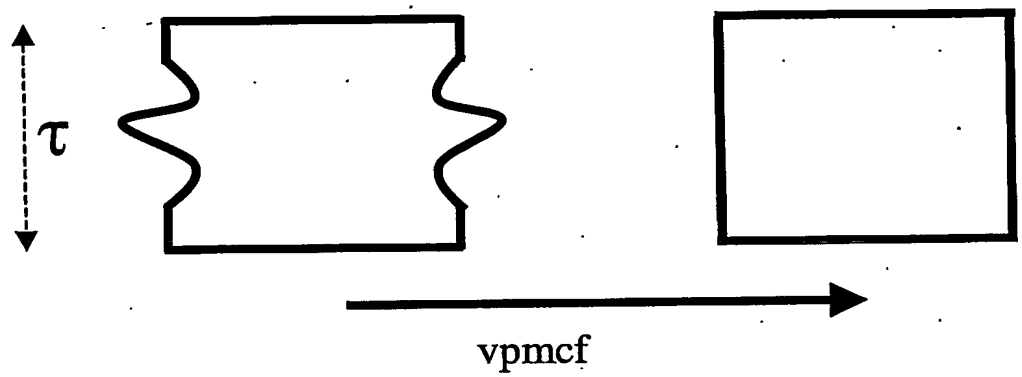

Figure 8

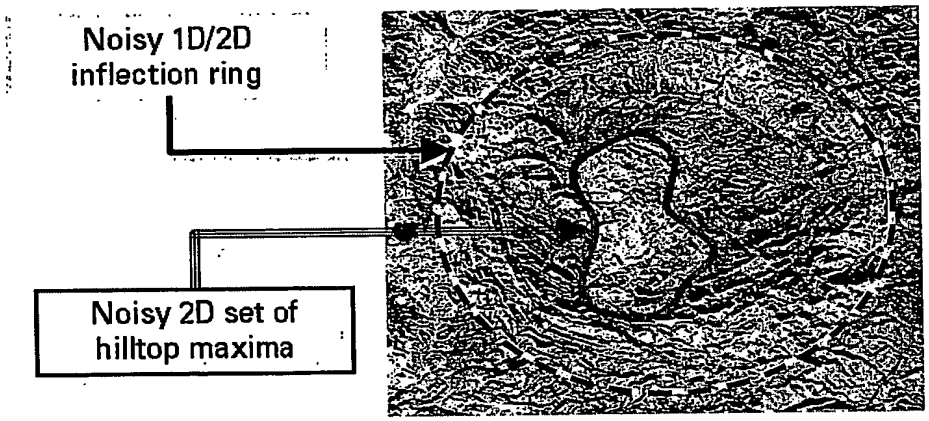

Figure 9

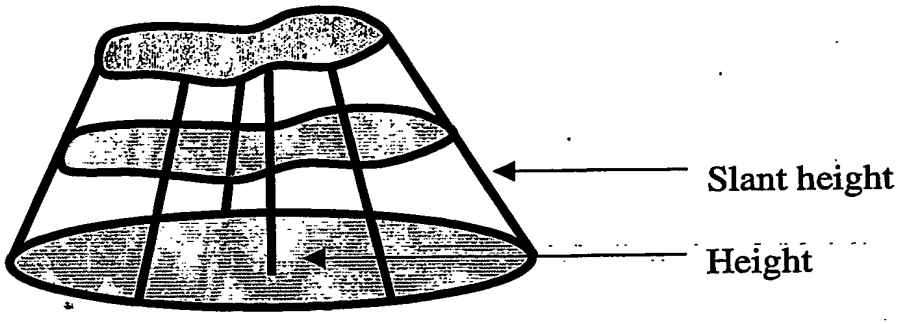

Figure 10

Figure 11

Figure 12

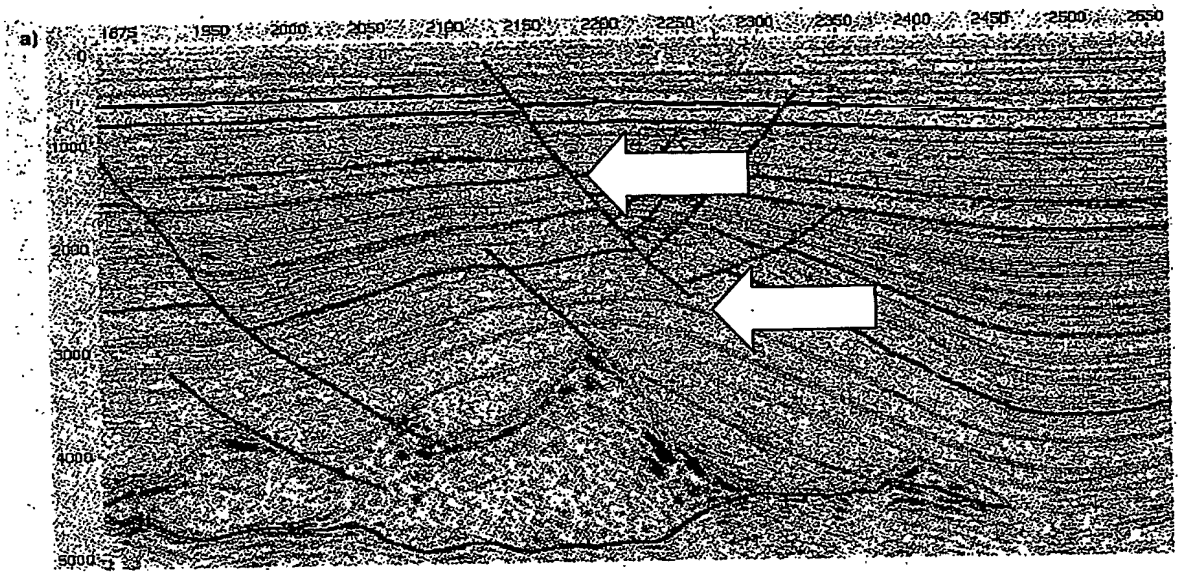

Figure 13

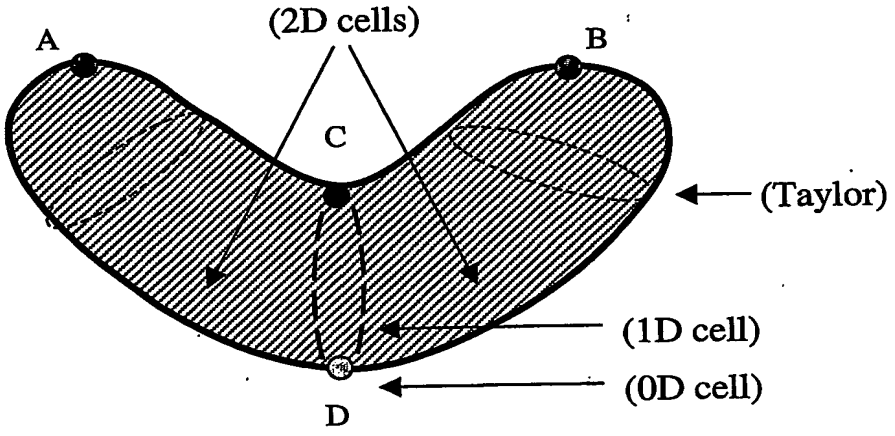

Figure 14

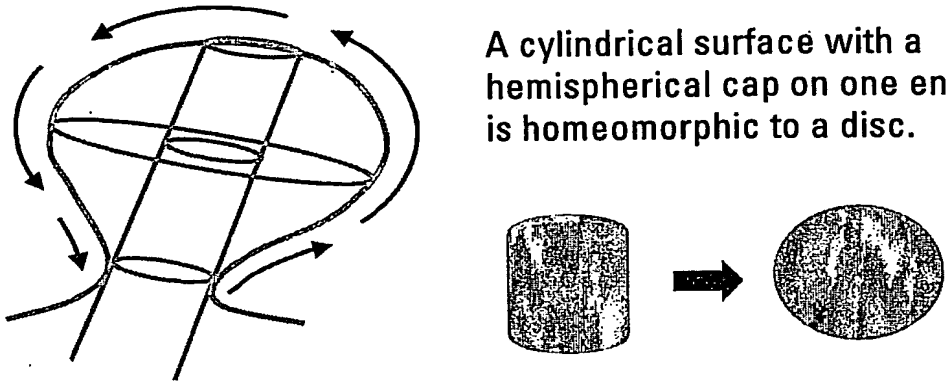

Figure 15

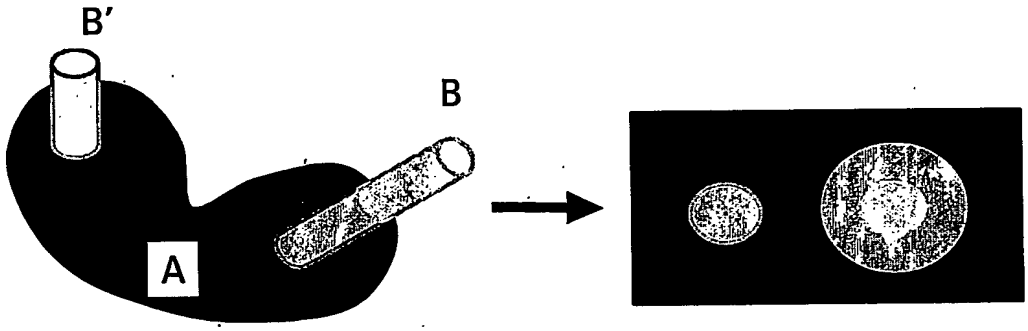

Figure 16

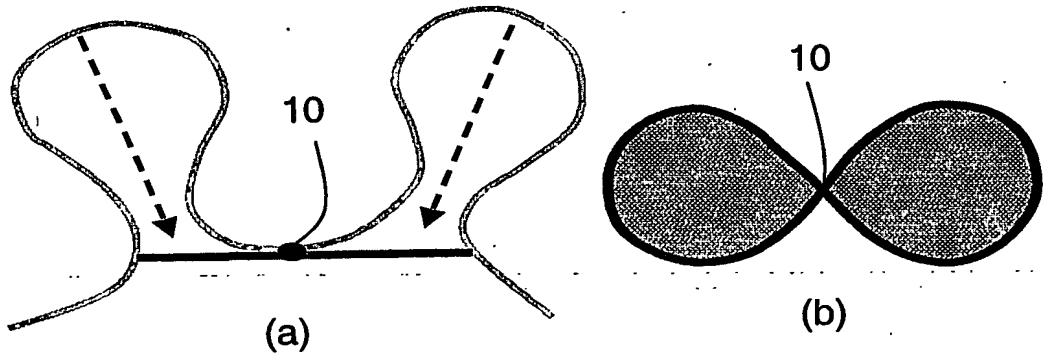

Figure 17

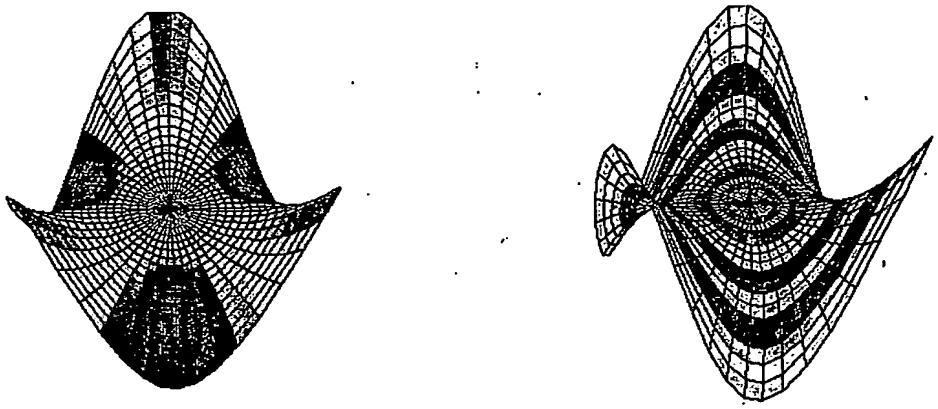

Figure 18

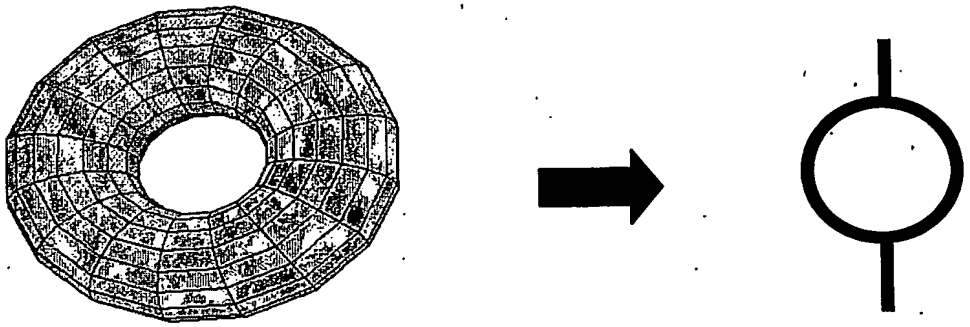

Figure 19

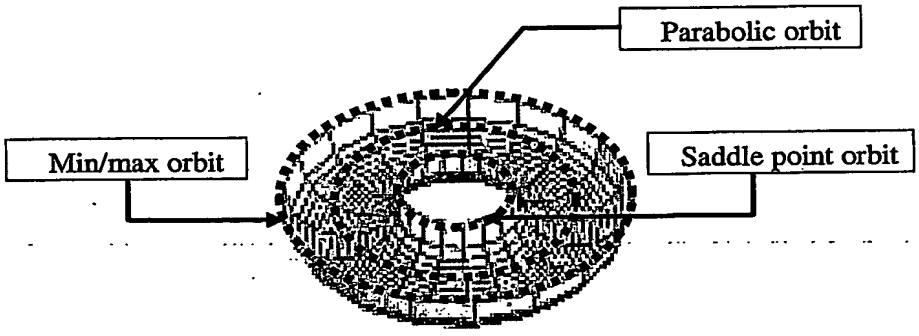

Figure 20

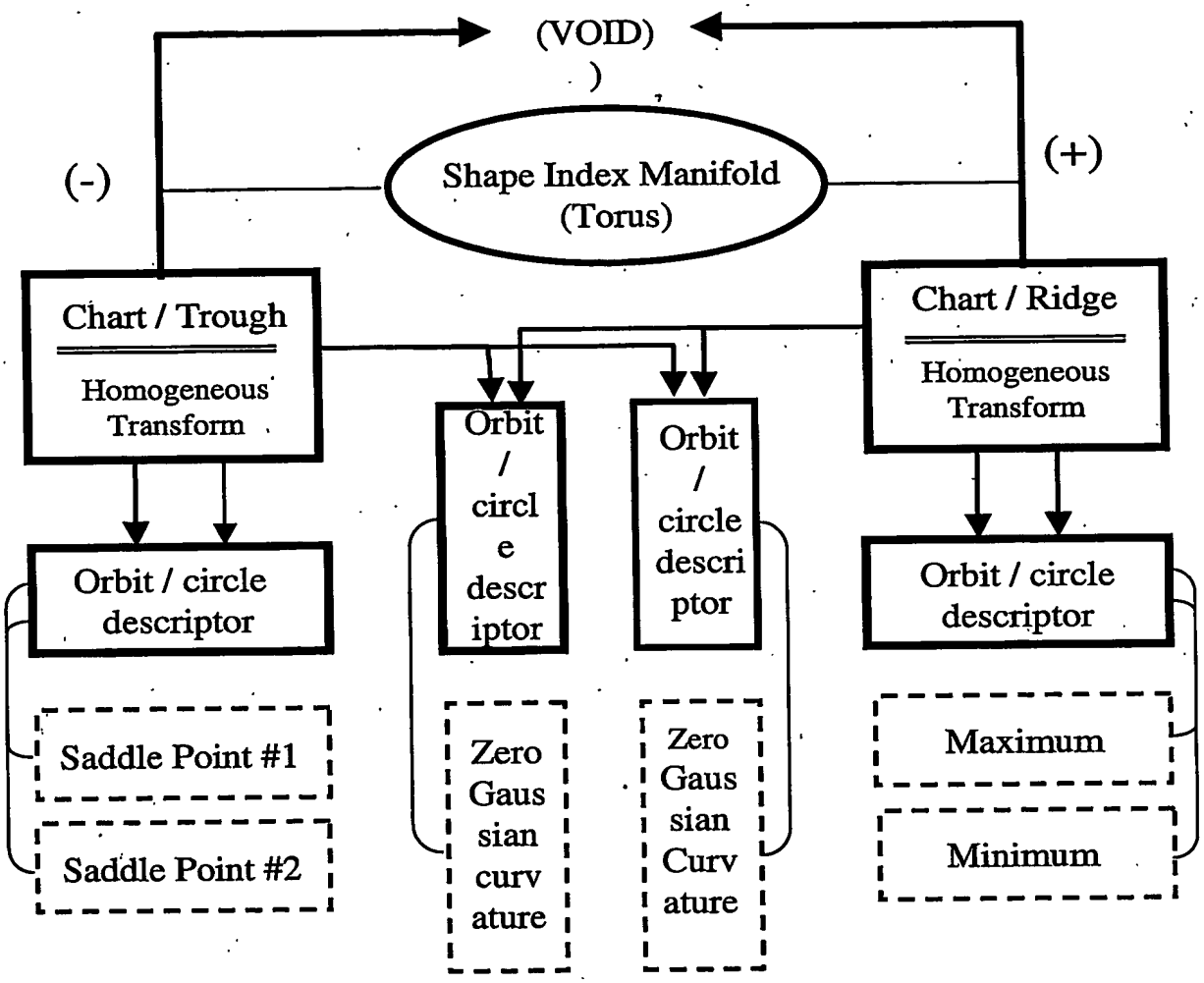
(VOID)
)
(-)
Shape Index Manifold
(Torus)
(+)
Chart / Trough
Homogeneous
Transform
Chart / Ridge
Homogeneous
Transform
Orbit / circle descriptor
Orbit / circle descriptor
Orbit / circle descriptor
Saddle Point #1
Saddle Point #2
Zero Gaussian curvature
Zero Gaussian Curvature
Maximum
Minimum

Figure 21

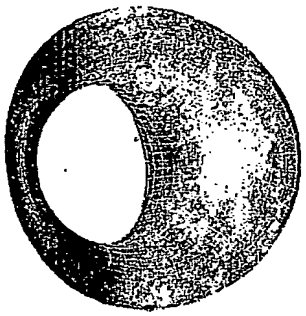

Figure 22

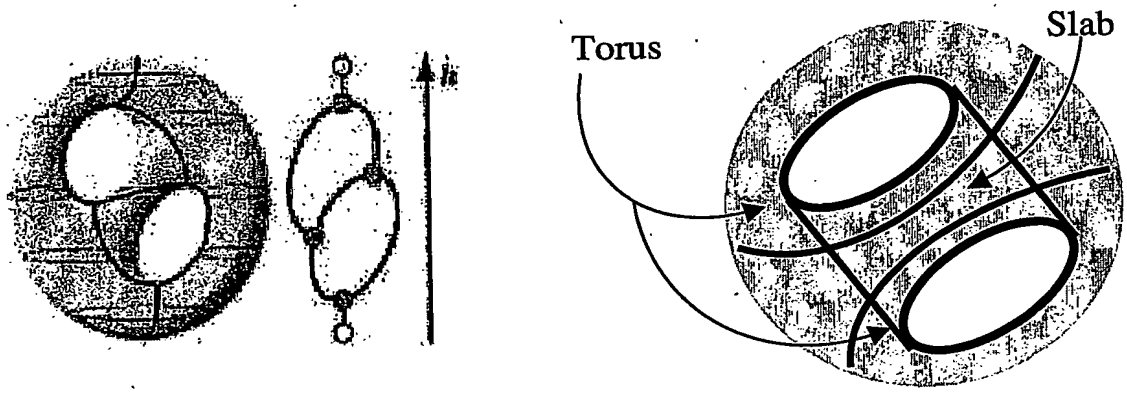

Figure 23

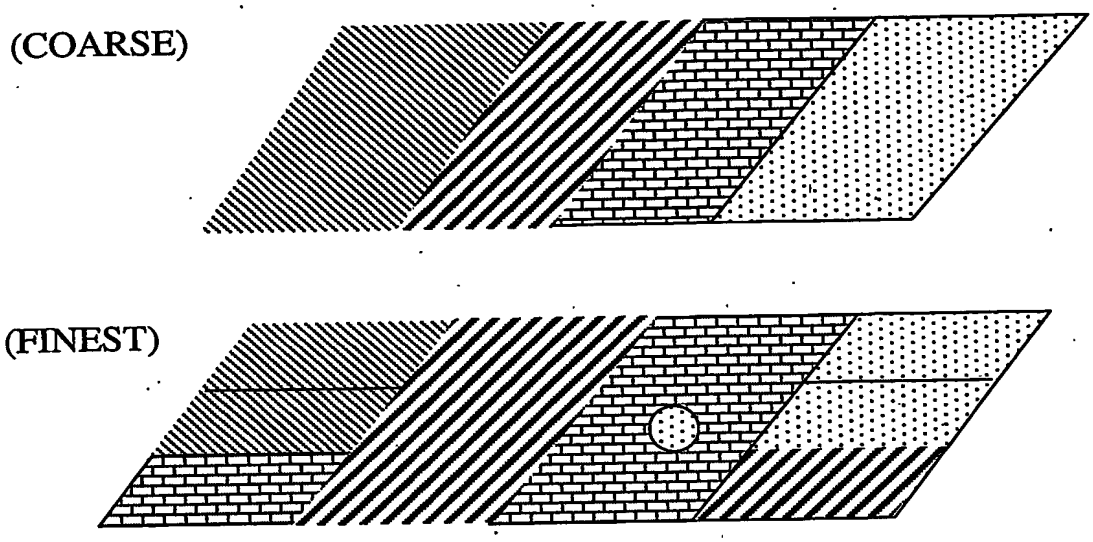

Figure 24

Stable shape index regions

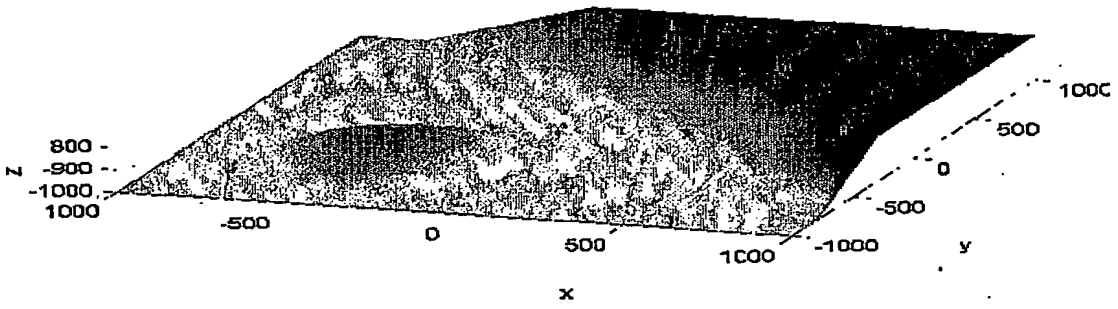

Figure 25

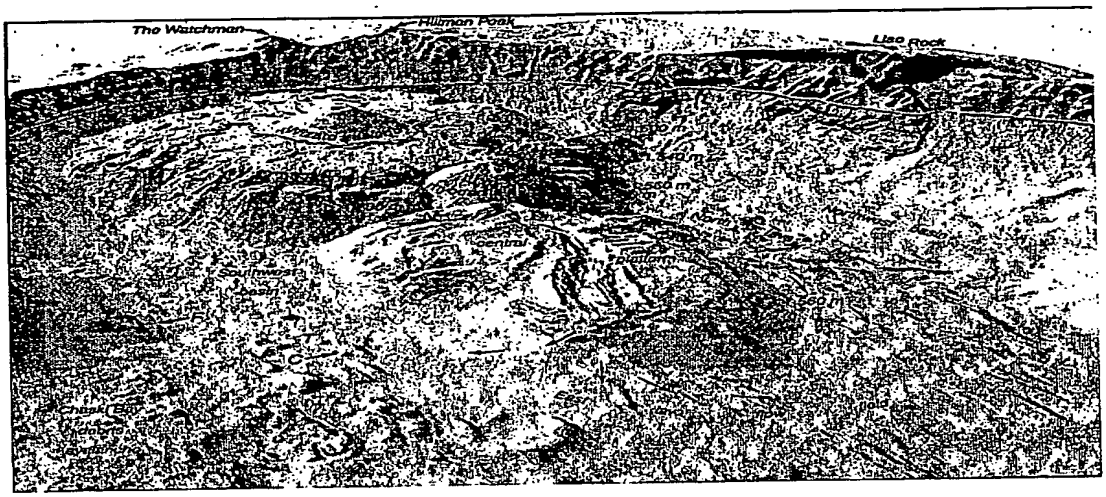

Figure 26

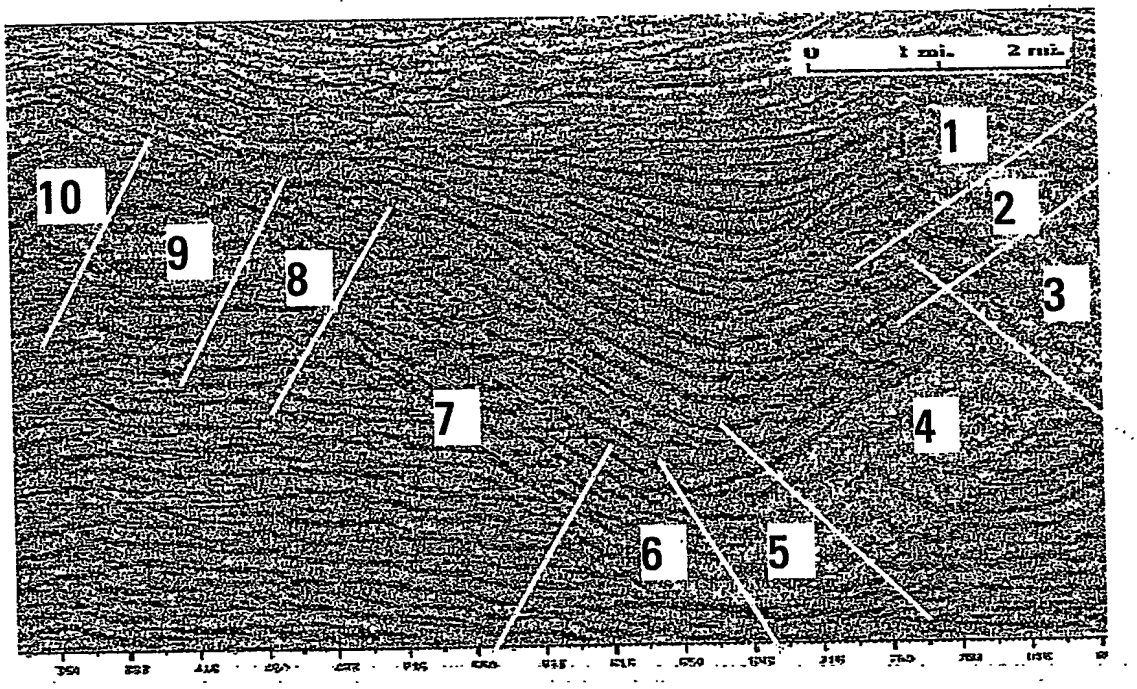

Figure 27

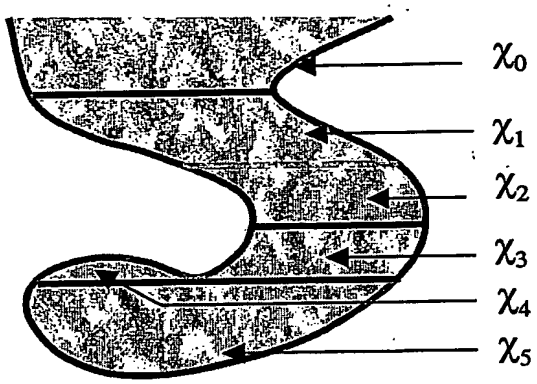

Figure 28a

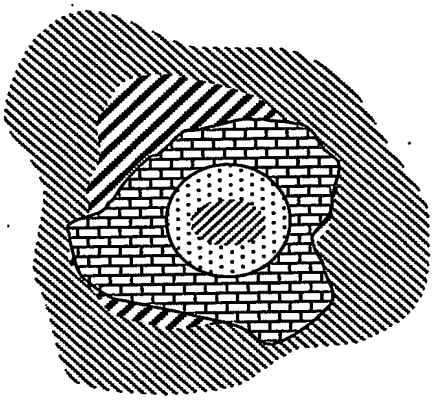

Figure 28b

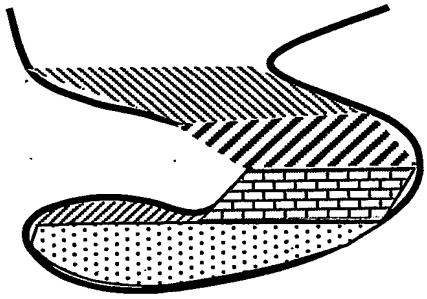

Figure 28c

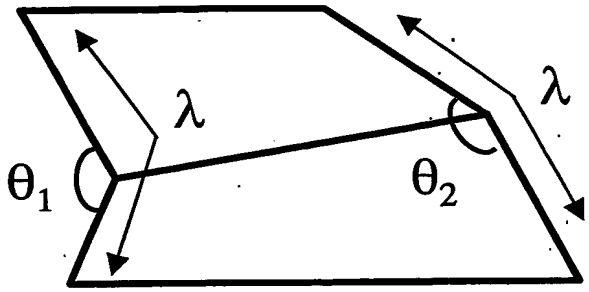

Figure 29a

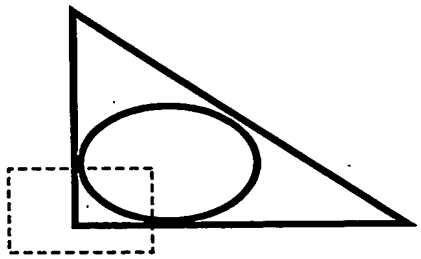

Figure 29b

$$Squeeze = \begin{pmatrix} \sin\vartheta & 0 \\ \cos\vartheta & 1 \end{pmatrix}, \quad where \quad 0 \le \vartheta < \pi,$$

$$Stretch = \begin{pmatrix} \sigma_x & 0 \\ 0 & \sigma_y \end{pmatrix}, \quad where \quad \sigma_x, \sigma_y > 0,$$

$$Blend = Stretch * Squeeze = \begin{pmatrix} \sigma_x \sin\vartheta & 0 \\ \sigma_y \cos\vartheta & \sigma_y \end{pmatrix}.$$

Figure 29c

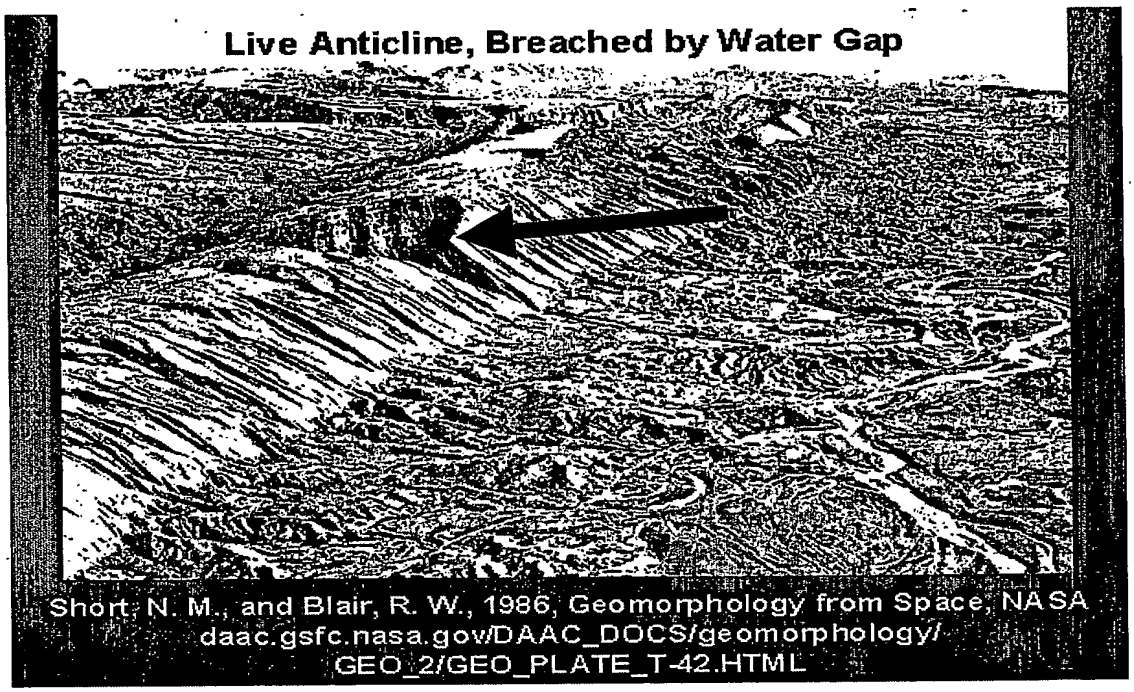

Figure 30

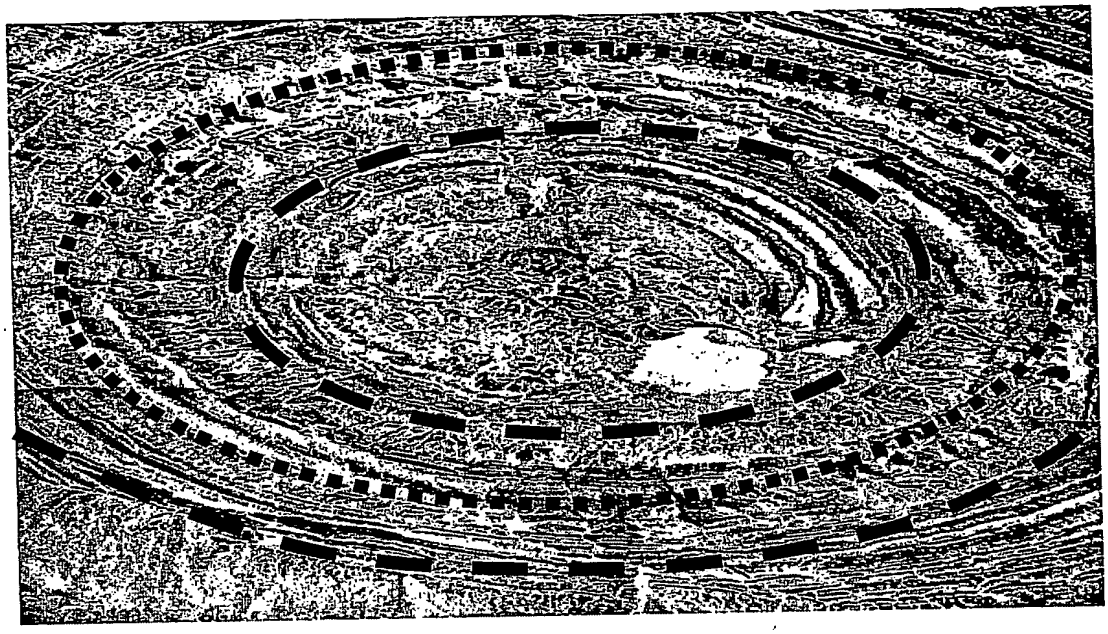

Figure 31

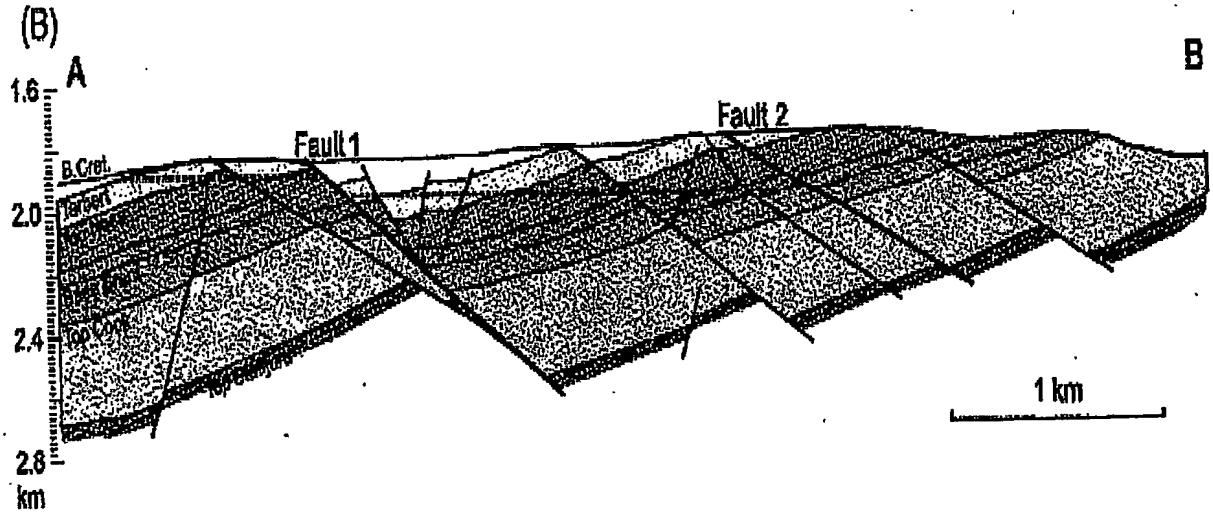

Figure 32

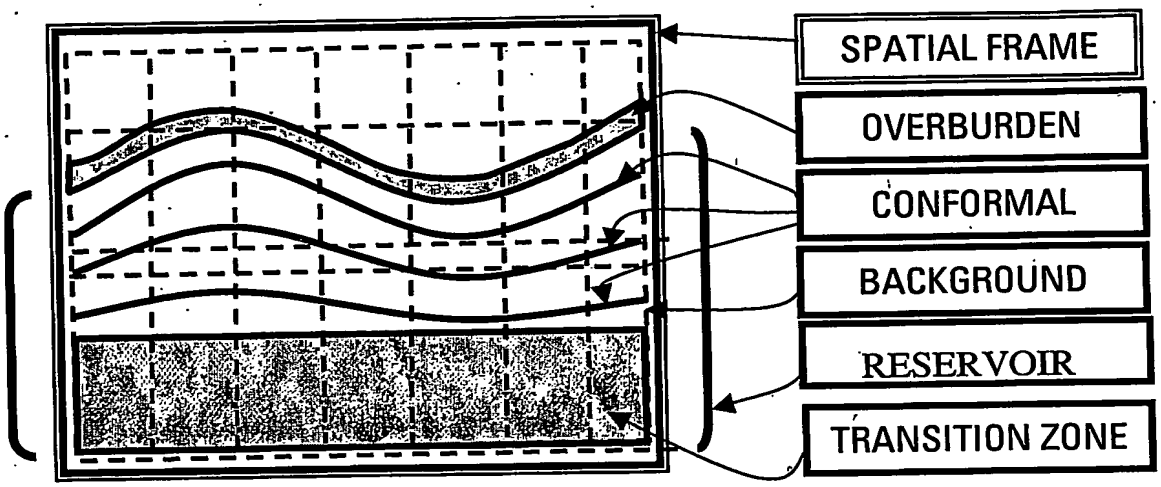

Figure 33

Figure 34

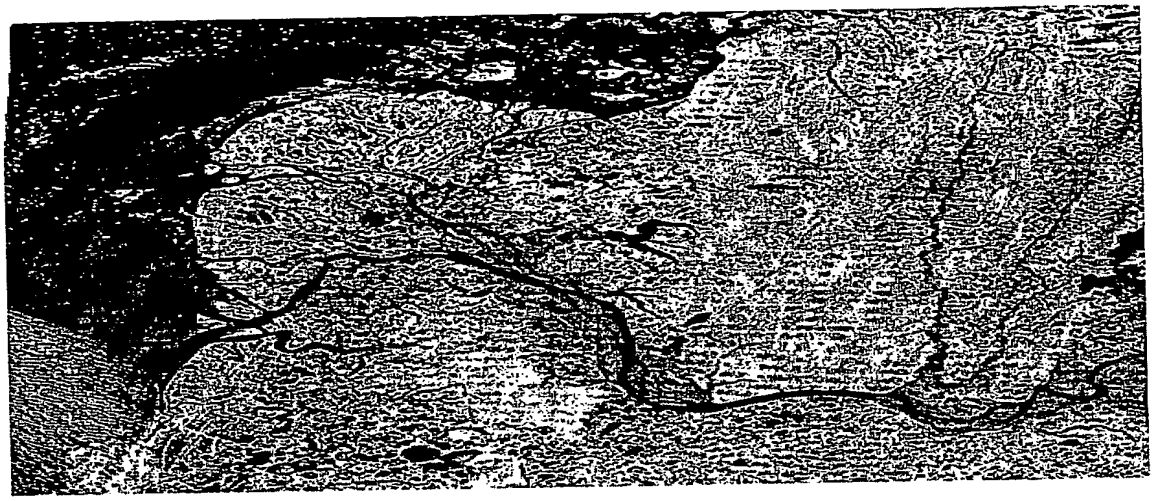

Figure 35

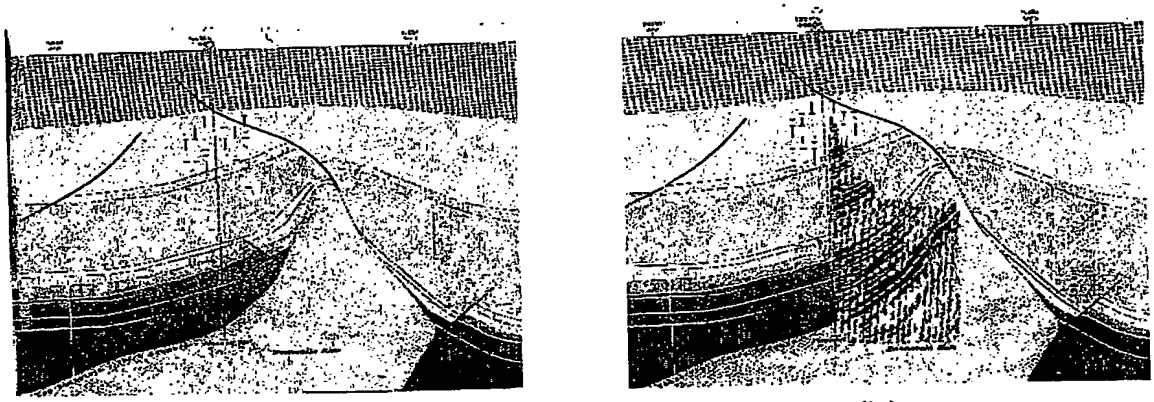

(a) (b)

Figure 36

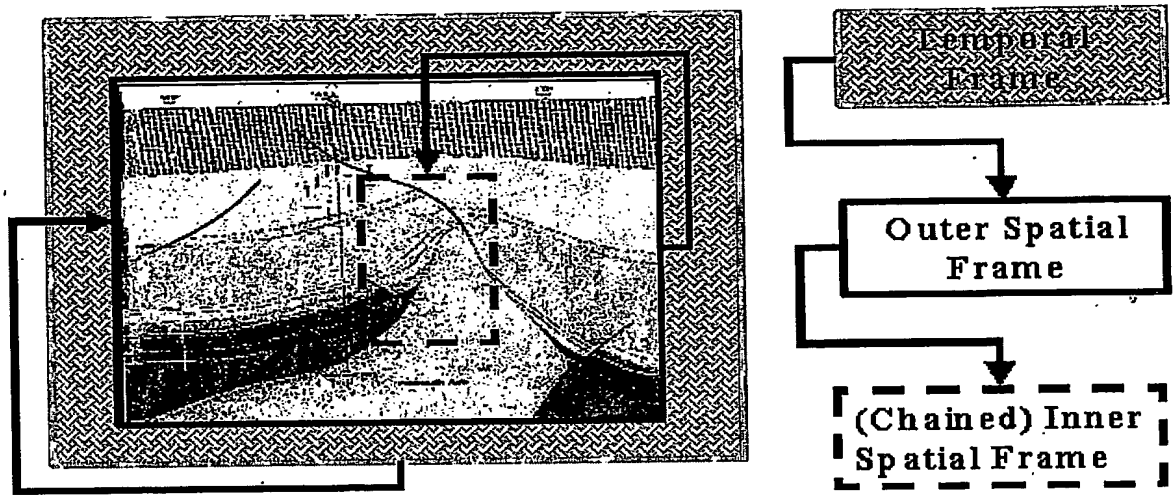

Figure 37

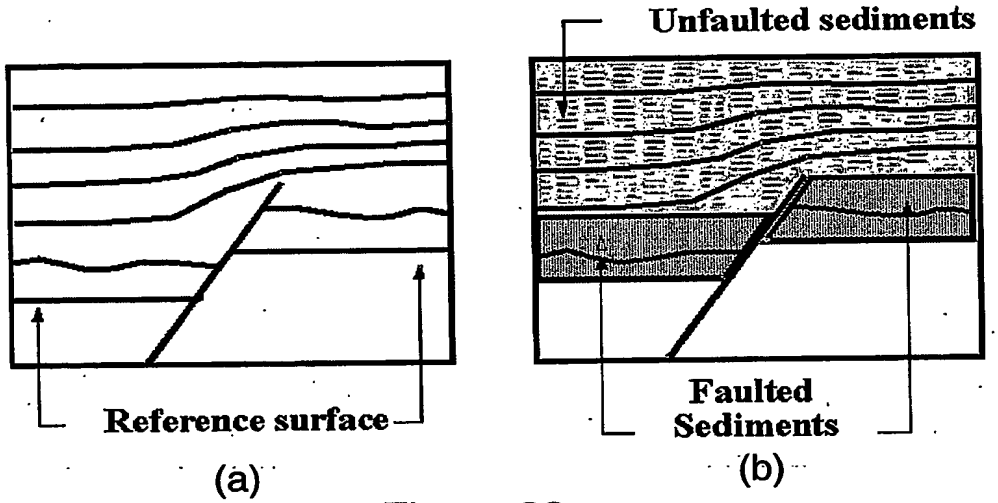

Figure 38

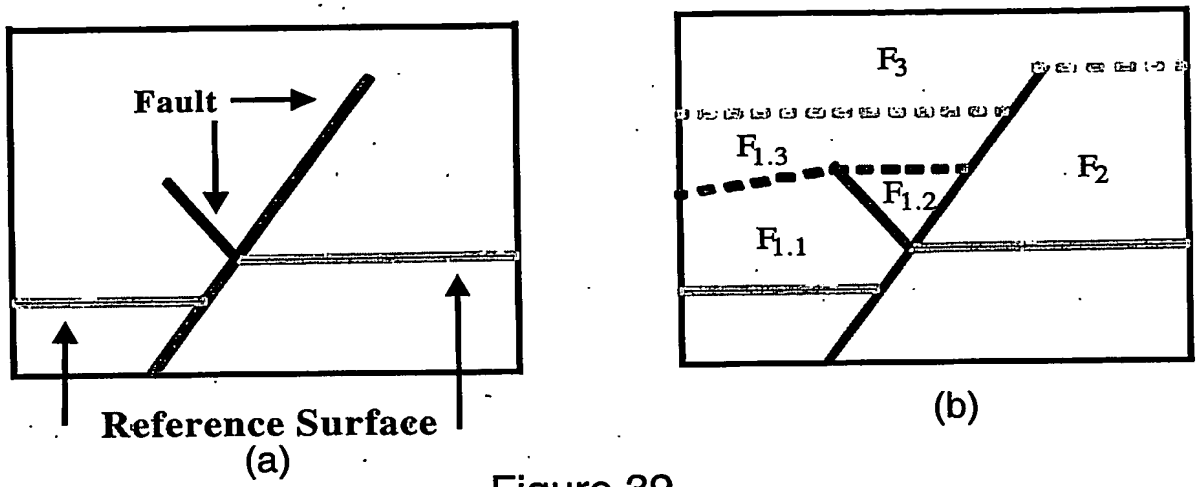

Figure 39

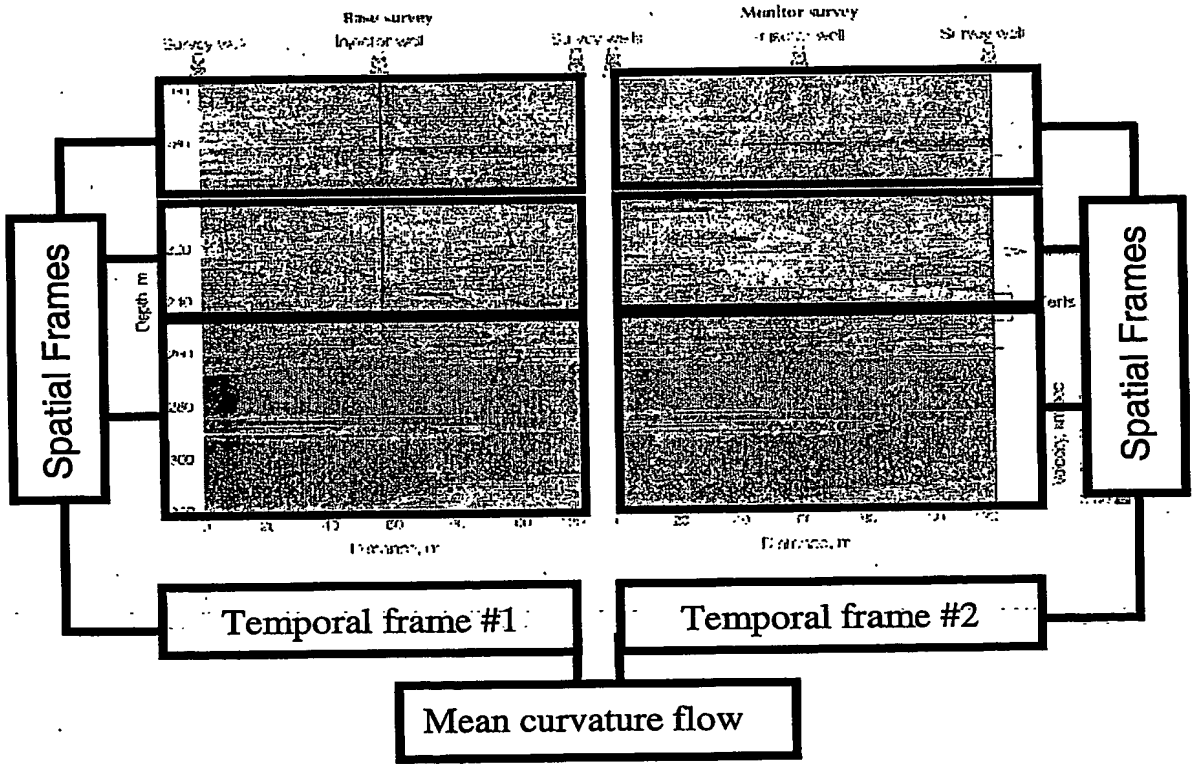

Figure 40

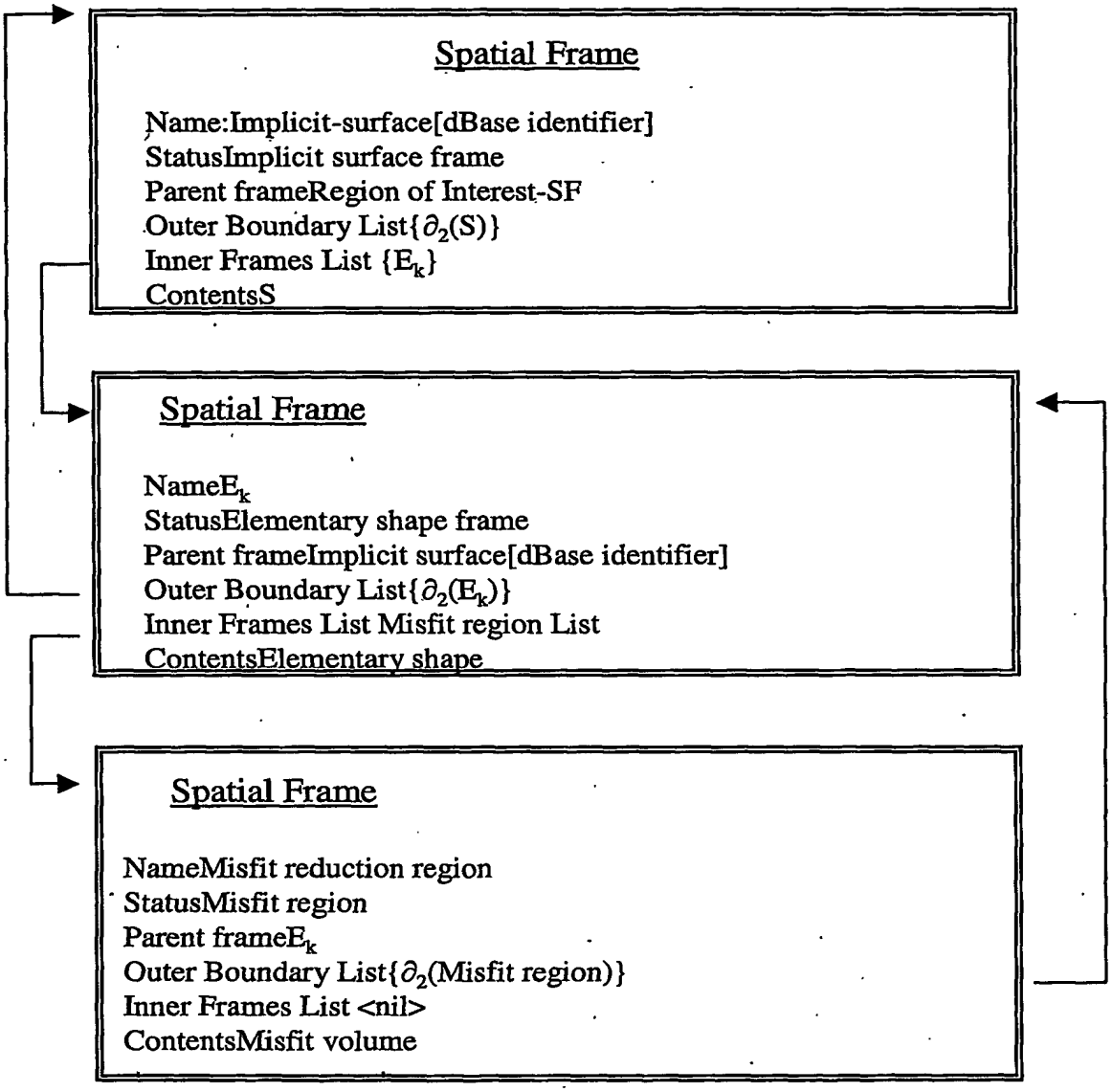
Spatial Frame
Name:Implicit-surface[dBase identifier]
StatusImplicit surface frame
Parent frameRegion of Interest-SF
Outer Boundary List{$\partial_2(S)$}
Inner Frames List {E_k}
ContentsS
Spatial Frame
NameE_k
StatusElementary shape frame
Parent frameImplicit surface[dBase identifier]
Outer Boundary List{$\partial_2(E_k)$}
Inner Frames List Misfit region List
ContentsElementary shape
Spatial Frame
NameMisfit reduction region
StatusMisfit region
Parent frameE_k
Outer Boundary List{∂_2(Misfit region)}
Inner Frames List <nil>
ContentsMisfit volume

Figure 41

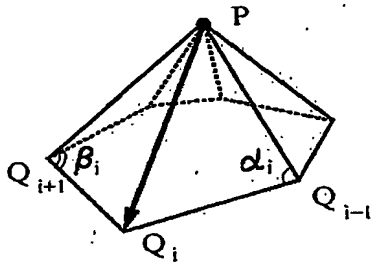

Figure 42

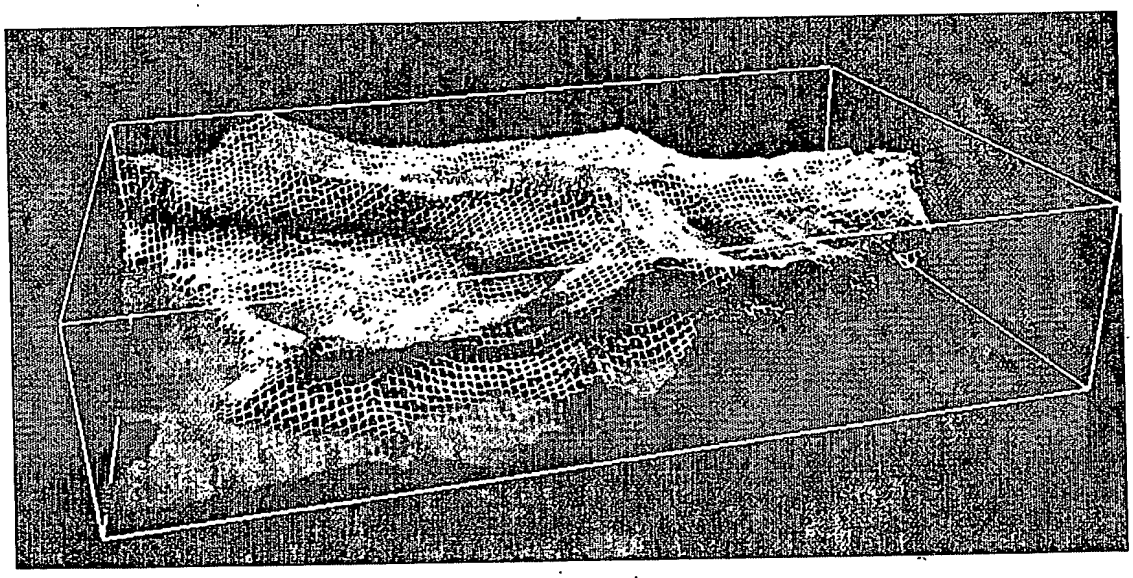

Figure 43

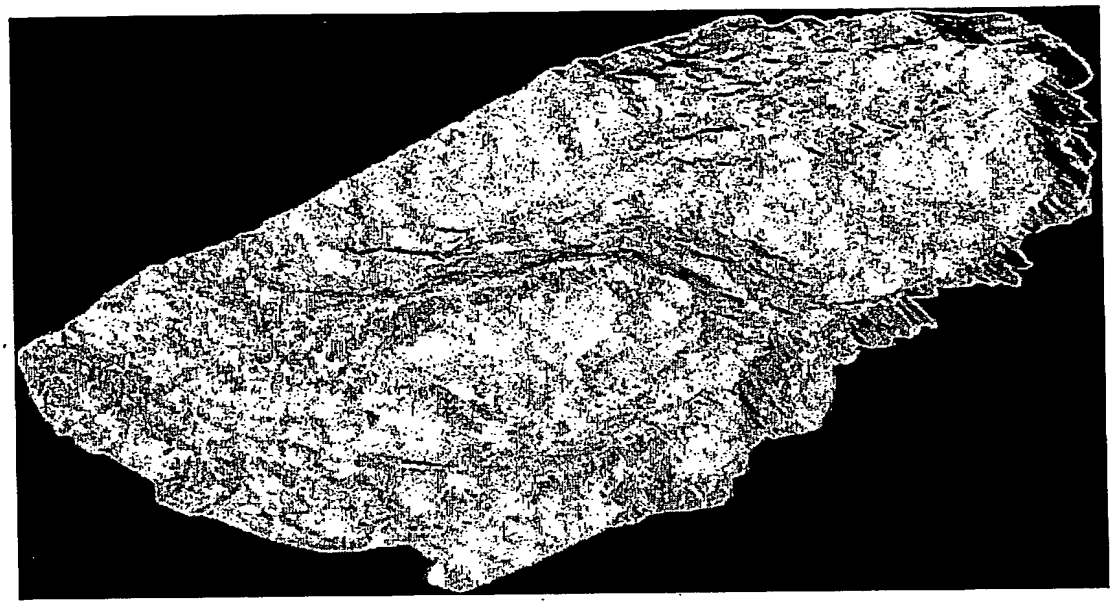

Figure 44

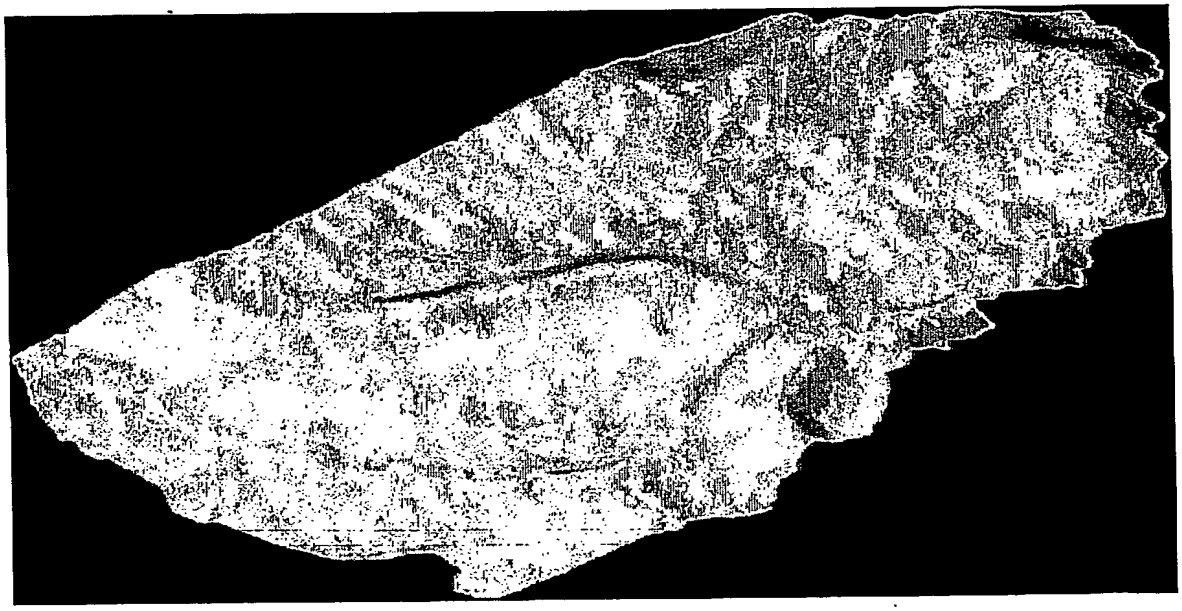

Figure 45

Figure 46

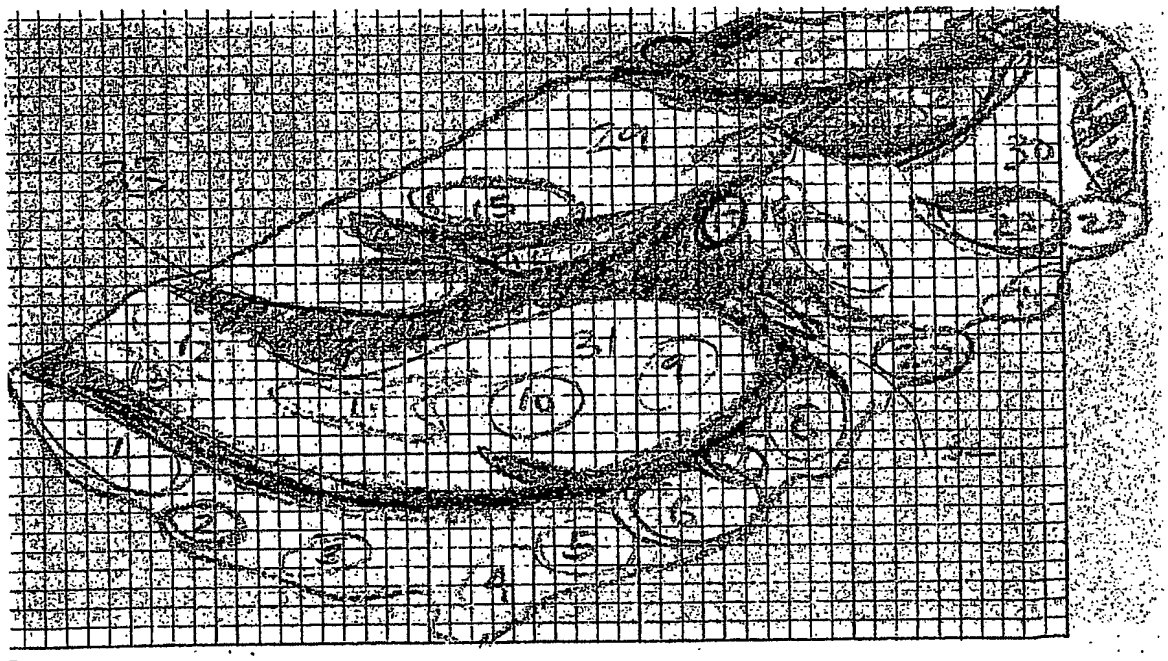

Figure 47

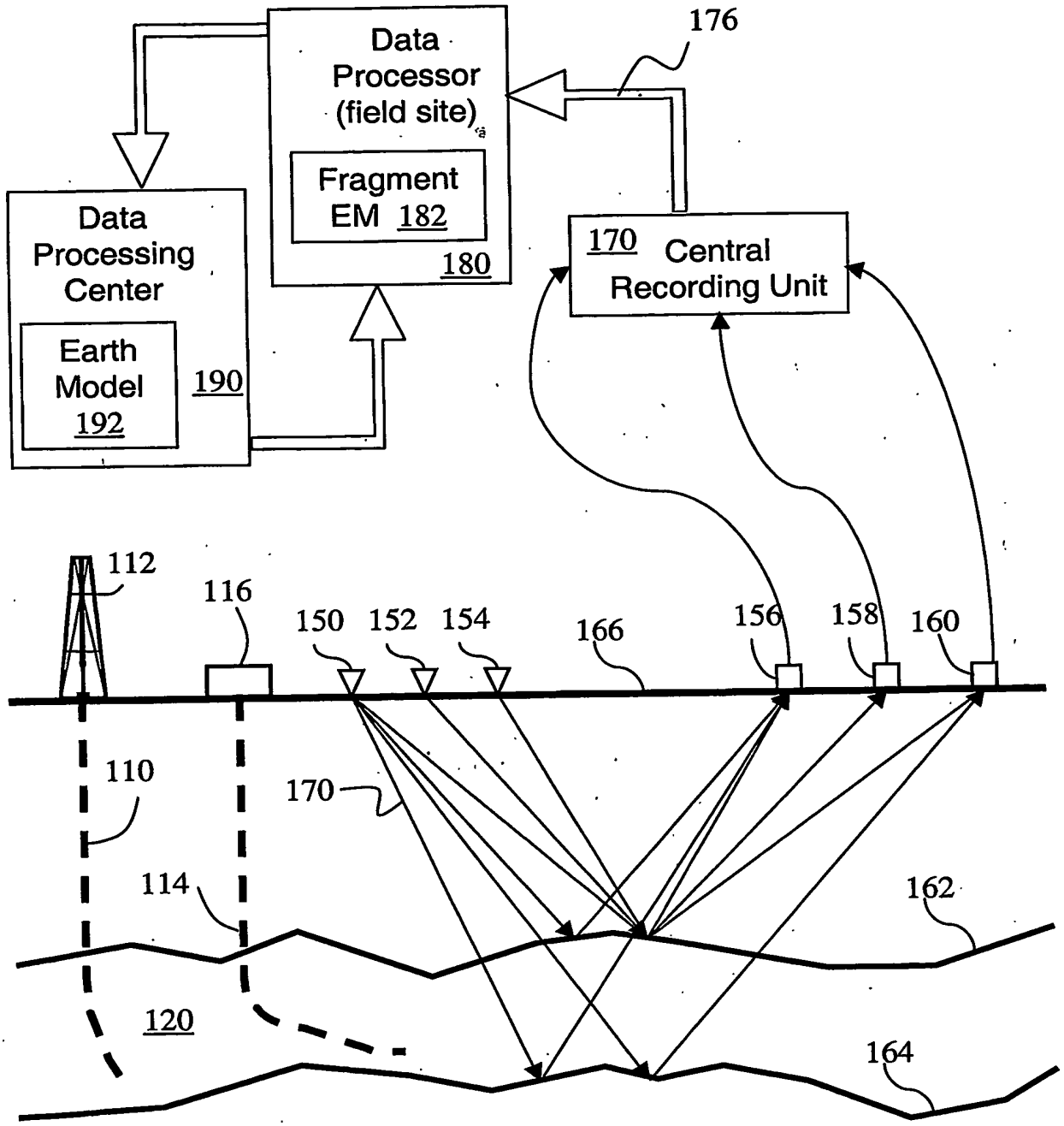
Data Processor (field site)
Fragment EM 182
180
176
Data Processing Center
Earth Model 192
190
170 Central Recording Unit
112
116
150
152
154
166
156
158
160
110
170
114
162
120
164

Figure 48

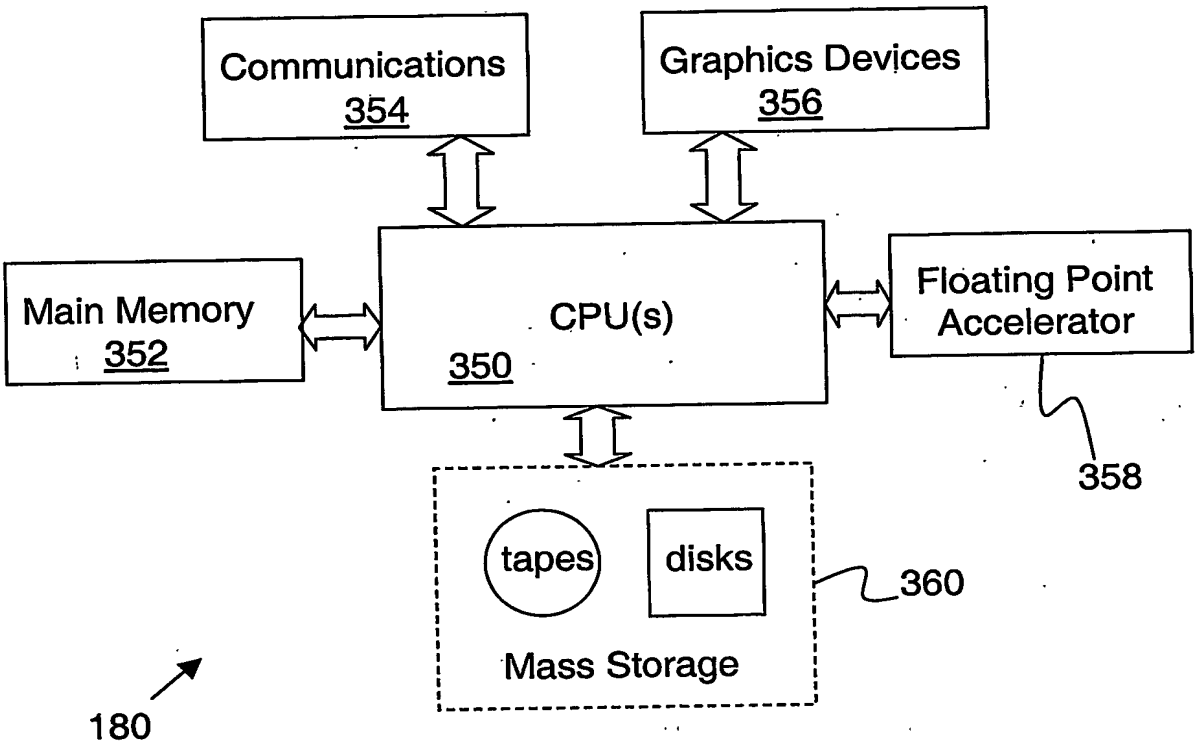
Communications
354
Graphics Devices
356
Main Memory
352
CPU(s)
350
Floating Point
Accelerator
358
tapes
disks
360
Mass Storage
180

Figure 49

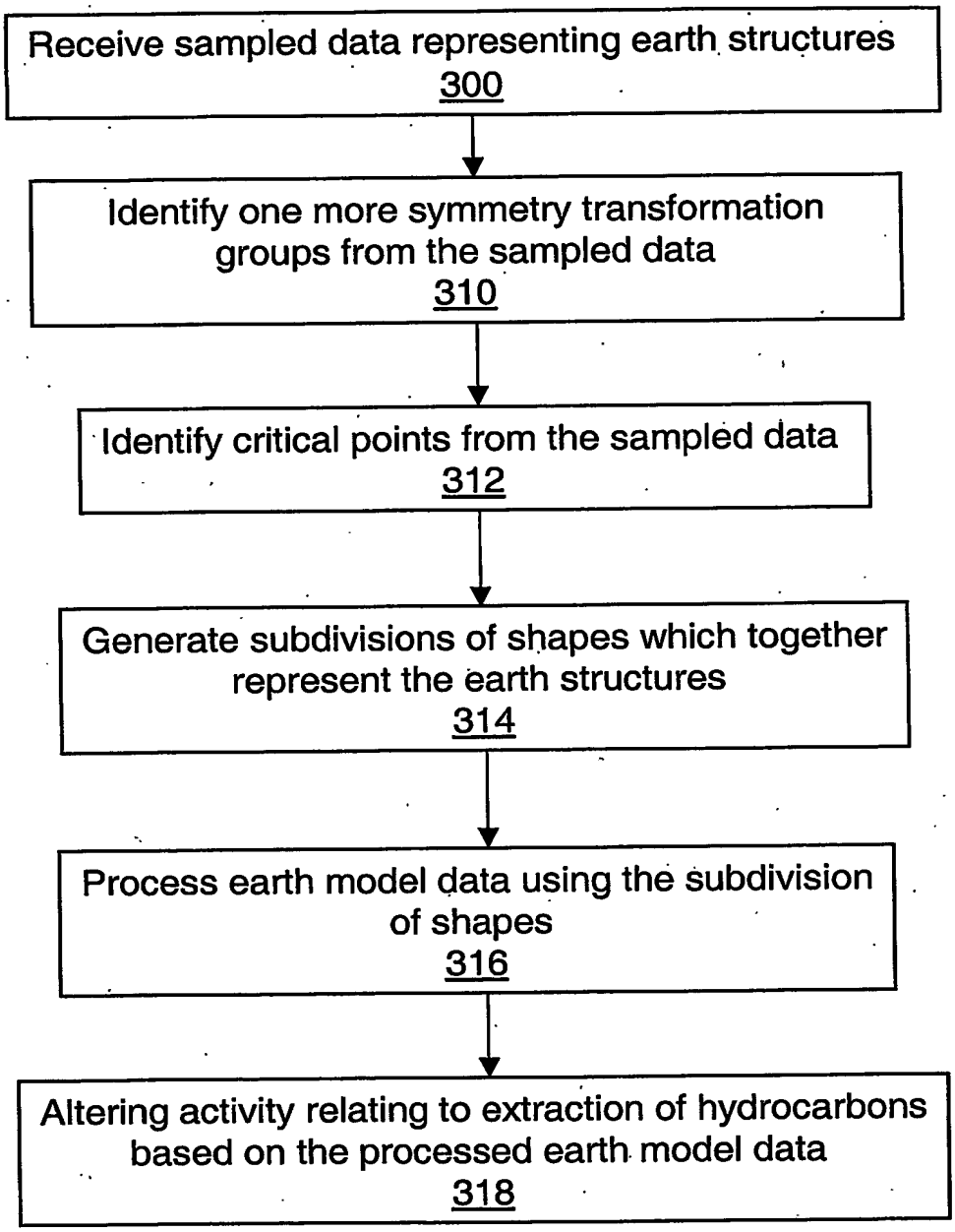
Receive sampled data representing earth structures
300
Identify one more symmetry transformation groups from the sampled data
310
Identify critical points from the sampled data
312
Generate subdivisions of shapes which together represent the earth structures
314
Process earth model data using the subdivision of shapes
316
Altering activity relating to extraction of hydrocarbons based on the processed earth model data
318

Figure 50

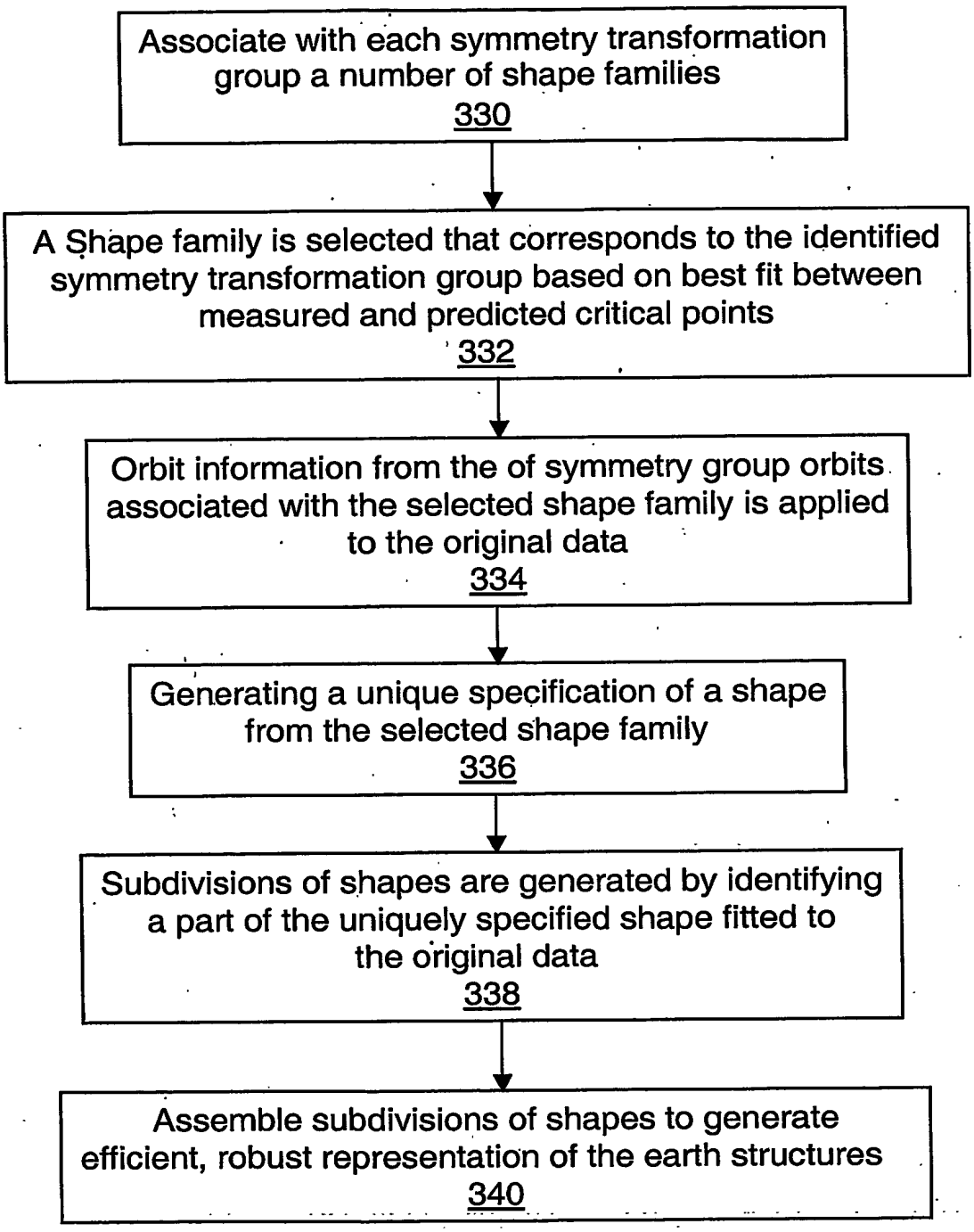
Associate with each symmetry transformation group a number of shape families
330
A Shape family is selected that corresponds to the identified symmetry transformation group based on best fit between measured and predicted critical points
332
Orbit information from the of symmetry group orbits associated with the selected shape family is applied to the original data
334
Generating a unique specification of a shape from the selected shape family
336
Subdivisions of shapes are generated by identifying a part of the uniquely specified shape fitted to the original data
338
Assemble subdivisions of shapes to generate efficient, robust representation of the earth structures
340

Figure 51

INTERNATIONAL SEARCH REPORT

Int. d Application No
PCT/GB 03/05395

A. CLASSIFICATION OF SUBJECT MATTER
IPC 7 G01V11/00

According to International Patent Classification (IPC) or to both national classification and IPC

B. FIELDS SEARCHED

Minimum documentation searched (classification system followed by classification symbols)
IPC 7 G01V

Documentation searched other than minimum documentation to the extent that such documents are included in the fields searched

Electronic data base consulted during the international search (name of data base and, where practical, search terms used)
EPO-Internal, WPI Data

C. DOCUMENTS CONSIDERED TO BE RELEVANT

Category °	Citation of document, with indication, where appropriate, of the relevant passages	Relevant to claim No.
A	WO 00/19380 A (SCHLUMBERGER CA LTD ;SCHLUMBERGER SERVICES PETROL (FR); SCHLUMBERG) 6 April 2000 (2000-04-06) cited in the application page 2, line 18 -page 3, line 20	1,36
A	US 6 323 863 B1 (SHINAGAWA YOSHIHISA ET AL) 27 November 2001 (2001-11-27) column 3, line 24 - line 56 column 6, line 4 -column 8, line 64	1,36
A	US 6 128 577 A (ASSA STEVEN BRENT ET AL) 3 October 2000 (2000-10-03) claim 1	1,36

☐ Further documents are listed in the continuation of box C.

☒ Patent family members are listed in annex.

° Special categories of cited documents:

'A' document defining the general state of the art which is not considered to be of particular relevance

'E' earlier document but published on or after the international filing date

'L' document which may throw doubts on priority claim(s) or which is cited to establish the publication date of another citation or other special reason (as specified)

'O' document referring to an oral disclosure, use, exhibition or other means

'P' document published prior to the international filing date but later than the priority date claimed

'T' later document published after the international filing date or priority date and not in conflict with the application but cited to understand the principle or theory underlying the invention

'X' document of particular relevance; the claimed invention cannot be considered novel or cannot be considered to involve an inventive step when the document is taken alone

'Y' document of particular relevance; the claimed invention cannot be considered to involve an inventive step when the document is combined with one or more other such documents, such combination being obvious to a person skilled in the art.

'&' document member of the same patent family

Date of the actual completion of the international search	Date of mailing of the international search report
2 June 2004	11/06/2004

Name and mailing address of the ISA	Authorized officer
European Patent Office, P.B. 5818 Patentlaan 2 NL – 2280 HV Rijswijk Tel. (+31-70) 340-2040, Tx. 31 651 epo nl, Fax: (+31-70) 340-3016	Lorne, B

Form PCT/ISA/210 (second sheet) (January 2004)

INTERNATIONAL SEARCH REPORT

Information on patent family members

I Application No
PCT/GB 03/05395

Patent document cited in search report	Publication date	Patent family member(s)	Publication date
WO 0019380 A	06-04-2000	US 6313837 B1	06-11-2001
		AU 765743 B2	25-09-2003
		AU 6500399 A	17-04-2000
		CA 2342351 A1	06-04-2000
		EP 1125254 A1	22-08-2001
		GB 2358570 A ,B	25-07-2001
		NO 20011572 A	28-05-2001
		WO 0019380 A1	06-04-2000
US 6323863 B1	27-11-2001	JP 3103793 B2	30-10-2000
		JP 10312472 A	24-11-1998
US 6128577 A	03-10-2000	CA 2275495 A1	25-06-1998
		EP 0992009 A1	12-04-2000
		WO 9827498 A1	25-06-1998